




# Molecular architecture of 40S translation initiation complexes on the hepatitis C virus IRES

Zuben P Brown<sup>1</sup> , Irina S Abaeva<sup>2</sup>, Swastik De<sup>1</sup>, Christopher U T Hellen<sup>2</sup> , Tatyana V Pestova<sup>2,\*</sup>  & Joachim Frank<sup>1,3,\*\*</sup> 

## Abstract

Hepatitis C virus mRNA contains an internal ribosome entry site (IRES) that mediates end-independent translation initiation, requiring a subset of eukaryotic initiation factors (eIFs). Biochemical studies revealed that direct binding of the IRES to the 40S ribosomal subunit places the initiation codon into the P site, where it base pairs with eIF2-bound Met-tRNA<sup>Met</sup> forming a 48S initiation complex. Subsequently, eIF5 and eIF5B mediate subunit joining, yielding an elongation-competent 80S ribosome. Initiation can also proceed without eIF2, in which case Met-tRNA<sup>Met</sup> is recruited directly by eIF5B. However, the structures of initiation complexes assembled on the HCV IRES, the transitions between different states, and the accompanying conformational changes have remained unknown. To fill these gaps, we now obtained cryo-EM structures of IRES initiation complexes, at resolutions up to 3.5 Å, that cover all major stages from the initial ribosomal association, through eIF2-containing 48S initiation complexes, to eIF5B-containing complexes immediately prior to subunit joining. These structures provide insights into the dynamic network of 40S/IRES contacts, highlight the role of IRES domain II, and reveal conformational changes that occur during the transition from eIF2- to eIF5B-containing 48S complexes and prepare them for subunit joining.

**Keywords** hepatitis C virus IRES; ribosome; eIF2; eIF5B; translation initiation

**Subject Categories** Structural Biology; Translation & Protein Quality

**DOI** 10.15252/embj.2022110581 | Received 5 January 2022 | Revised 1 June 2022 | Accepted 14 June 2022 | Published online 13 July 2022

**The EMBO Journal (2022) 41: e110581**

## Introduction

The canonical initiation process begins with formation of the 43S preinitiation complex (PIC) comprising the 40S ribosomal subunit, the eIF2-GTP/Met-tRNA<sup>Met</sup> ternary complex (eIF2-TC), eIF1, eIF1A, and eIF3 (Jackson *et al*, 2010). The 43S PIC attaches to the capped 5'-terminal region of mRNA and then scans to the initiation codon

in a favorable nucleotide context (containing A/G and G at the –3 and +4 positions relative to the AUG, respectively) where it stops and forms the 48S initiation complex (IC) with established codon–anticodon base pairing. Attachment is mediated by eIFs 4A, 4B, and eIF4F, which cooperatively unwind the cap-proximal region allowing attachment and also assist 43S PIC scanning. eIF1, in cooperation with eIF1A, stabilizes an “open” scanning-competent conformation of the 43S PIC and monitors the fidelity of initiation codon selection (Pestova *et al*, 1998a; Pestova & Kolupaeva, 2002; Passmore *et al*, 2007; Hussain *et al*, 2014). Establishment of codon–anticodon base pairing in the 48S IC leads to dissociation of eIF1 and eIF5-induced hydrolysis of eIF2-bound GTP, and thereby switches the 40S subunit to the “closed” conformation (Unbehauen *et al*, 2004; Maag *et al*, 2005). After that, eIF5B, in its GTP-bound form, displaces residual eIF2-GDP (Pisarev *et al*, 2006) and promotes the joining of the 60S subunit (Pestova *et al*, 2000). Interaction of eIF5B with eIF1A enhances eIF5B’s subunit joining activity and the hydrolysis of eIF5B-bound GTP, leading to the coupled release of eIF5B-GDP and eIF1A from the assembled 80S ribosome (Marintchev *et al*, 2003; Acker *et al*, 2006; Nag *et al*, 2016).

A number of viral mRNAs contain internal ribosomal entry sites (IRESs), structured RNA regions that mediate cap-independent initiation of translation using only a subset of the eIFs that are required by canonical initiation. All IRES-mediated initiation mechanisms are based on noncanonical interactions of IRESs with canonical components of the translation apparatus (Jackson *et al*, 2010). The ~300-nt-long hepatitis C virus (HCV) IRES is located in the 5'-terminal region of the viral genome and epitomizes a class of related RNA elements. HCV-like IRESs occur in the genomes of pestiviruses (e.g., classical swine fever virus (CSFV)), some pegiviruses and caliciviruses, and numerous members of *Picornaviridae* (Arhab *et al*, 2020, 2022). The HCV IRES comprises two major domains (II–III), with domain III divided into several subdomains (Fig 1A). Ribosomal recruitment of HCV and HCV-like IRESs occurs by direct binding of the IRES to the 40S subunit and does not involve scanning, group 4 eIFs, or eIF1 (Pestova *et al*, 1998b). Domain III binds at the back of the 40S subunit, whereas the long, bent domain II loops out and reaches into the E site. The sites of interaction with the 40S subunit include domains IIIa and IIIc (which bind to eS1, eS26, and

<sup>1</sup> Department of Biochemistry and Molecular Biophysics, Columbia University, New York, NY, USA

<sup>2</sup> Department of Cell Biology, SUNY Downstate Health Sciences University, Brooklyn, NY, USA

<sup>3</sup> Department of Biological Sciences, Columbia University, New York, NY, USA

\*Corresponding author. Tel: +1 718 270 1034; E-mail: tatyana.pestova@downstate.edu

\*\*Corresponding author (Lead contact). Tel: +1 212 305 9512; E-mail: jf2192@cumc.columbia.edu

eS27), the apex of domain III<sub>d</sub> (which base pairs to expansion segment (ES) 7 of 18S rRNA), domain III<sub>e</sub> (which interacts with helix (h) 26 of 18S rRNA), and the apex of domain II, which interacts with uS7 and eS25 in the head and uS11 on the platform of the 40S subunit, intercalating into the mRNA-binding channel, and causing tilting of the head and forcing the 40S subunit to adopt the open conformation (Kolupaeva *et al*, 2000; Kieft *et al*, 2001; Hashem *et al*, 2013; Malygin *et al*, 2013a, 2013b; Matsuda & Mauro, 2014; Quade *et al*, 2015; Yamamoto *et al*, 2015; Angulo *et al*, 2016; Yokoyama *et al*, 2019).

Although domain II does not contribute to the affinity of the HCV IRES to the 40S subunit (e.g., Kieft *et al*, 2001; Spahn *et al*, 2001), the open conformation of the 40S subunit promoted by domain II facilitates loading of the region containing the initiation codon into the mRNA-binding channel, accounting for the stimulatory role of domain II during initiation on HCV-like IRESs (Honda *et al*, 1996; Reynolds *et al*, 1996; Odreman-Macchioli *et al*, 2001; Filbin & Kieft, 2011). Upon binding to the 40S subunit, the initiation codon is placed in the immediate vicinity of the P site, where it base pairs with the anticodon of Met-tRNA<sub>i</sub><sup>Met</sup> as a part of the eIF2-TC, leading to the formation of the 48S IC (Pestova *et al*, 1998b). After that, eIF5 and eIF5B mediate the subunit joining step to complete the formation of the elongation-competent 80S ribosome (Locker *et al*, 2007; Pestova *et al*, 2008; Terenin *et al*, 2008). Notably, in 80S complexes assembled on the HCV IRES, the P-site Met-tRNA<sub>i</sub><sup>Met</sup>, and eIF5B-GTP, which correspond to the last stage in the initiation process prior to the formation of an elongation-competent ribosome, the tilt of the 40S subunit is reversed, and the apex of domain II is released from its position on the head of the 40S subunit (Yamamoto *et al*, 2014). Remarkably, when levels of active eIF2 are reduced due to stress-induced phosphorylation, Met-tRNA<sub>i</sub><sup>Met</sup> can be recruited by eIF5B instead of the IRES/40S complexes (Pestova *et al*, 2008; Terenin *et al*, 2008). In both eIF2- and eIF5B-mediated pathways, eIF1A enhances 48S complex formation (de Breyne *et al*, 2008; Jaafar *et al*, 2016), whereas eIF1 inhibits the process and even induces dissociation of preassembled 48S ICs, but this inhibition can be alleviated by deletion of domain II (Pestova *et al*, 2008).

In addition to 40S subunits, HCV and related IRESs also bind to eIF3 via their apical III<sub>a</sub> and III<sub>b</sub> domains (Sizova *et al*, 1998; Pestova *et al*, 1998b; Ji *et al*, 2004; Hashem *et al*, 2013). Strikingly, in 40S/IRES/eIF3 complexes, HCV-like IRESs displace eIF3 from its ribosomal position (Hashem *et al*, 2013), usurping eIF3's key ribosomal contacts involving eS1, eS26, and eS27 (des Georges *et al*, 2015). Moreover, the ribosome-binding surface of eIF3 is now involved in interaction with the IRES (Hashem *et al*, 2013). In *in vitro* reconstituted initiation reactions, eIF3 only modestly enhances 48S complex formation on HCV-like IRESs (Pestova *et al*, 1998b; Hashem *et al*, 2013), which led to the suggestion that *in vivo*, the role of the eIF3/IRES interaction is likely to relieve the competition between the IRES and eIF3 for a common ribosomal binding site, and to reduce the formation of 43S PICs, thereby favoring translation of viral mRNAs (Hashem *et al*, 2013).

Cryo-EM studies have been indispensable in providing insights into the architecture and interactions of HCV and HCV-like IRES ribosomal complexes, and the mechanism of the IRES function, initially through low-resolution 40S/HCV IRES and 80S/HCV IRES

structures (Spahn *et al*, 2001; Boehringer *et al*, 2005) and continuing with sub-nanometer resolution structures of 40S/eIF3/CSFV IRES and 80S/Met-tRNA<sub>i</sub><sup>Met</sup>/eIF5B-GMPPNP/HCV IRES functional complexes (Hashem *et al*, 2013; Yamamoto *et al*, 2014), and the more recent near-atomic resolution reconstructions of 80S-HCV IRES complexes (Quade *et al*, 2015; Yamamoto *et al*, 2015; Yokoyama *et al*, 2019). However, despite these advances, the structures of 48S ICs assembled on the HCV IRES, and the transitions between different states in the initiation pathways and accompanying conformational changes have remained unknown. To fill these gaps, we present cryo-EM structures of HCV IRES ribosomal complexes up to 3.5 Å resolution that cover all major stages of IRES-mediated initiation pathways, from IRES binding to the 40S subunit through eIF2-containing 48S ICs to the final eIF5B-containing 48S ICs immediately prior to the joining of the 60S subunit. Individually, these structures also provide detailed insights into the dynamic network of contacts between the IRES and the 40S subunit, highlight the role of IRES domain II, and importantly, include the first structure of eIF5B bound to the 40S subunit, prior to subunit joining.

## Results

### Overview of cryo-EM analysis of initiation complexes assembled on the wt and the ΔII HCV IRES with eIF2 or eIF5B

To capture discrete states in the eIF2- and the eIF5B-mediated initiation pathways on the HCV IRES and to visualize the role of IRES domain II in these processes, initiation complexes were reconstituted *in vitro* by incubating the wt or the ΔII mutant IRES (Fig 1A) with individual purified translation components. To follow the eIF2-mediated pathway, assembly mixtures contained the wt or the ΔII IRES, 40S subunits, eIF2, eIF3, eIF1A, and Met-tRNA<sub>i</sub><sup>Met</sup>, and to follow the eIF5B-mediated pathway, eIF2 was replaced by eIF5B, thus yielding four discrete sample types (Appendix Table S1). Cryo-EM grids of each complex were imaged at 300 kV producing high-contrast micrographs with easily identifiable 40S ribosomal particles (Appendix Fig S1A–E and Table S2). The images were processed using maximum-likelihood classification techniques implemented in Relion 3.1 (Scheres, 2012, 2016; Zivanov *et al*, 2018, 2019), yielding 18 structures containing different sets of components at resolutions as high as 3.5 Å (Figs 1B and EV1A, Appendix Figs S1F and G, and S2, Table S3). Although some flexible regions had a poor local resolution (e.g., eS12 in the 40S head or IRES domain III<sub>b</sub>), most of the ribosomes, all IRES-ribosome contacts, and all initiation factors present had resolutions, between 3–7 Å (Appendix Figs S2 and S3A–F), that allowed modeling of these components. None of the structures obtained contained eIF3. During initiation on HCV-like IRESs, eIF3 interacts with the apical region of IRES domain III rather than with the 40S subunit (Hashem *et al*, 2013). This interaction is sensitive to the process of grid preparation and is more stable when grids have thicker ice, so that imaging complexes that contain eIF3 require the intentional selection of regions with sufficiently thick ice (e.g., Hashem *et al*, 2013; Neupane *et al*, 2020); however, our study aimed to determine the details of ribosomal interactions with the IRES, initiation factors, and Met-tRNA<sub>i</sub><sup>Met</sup> at high resolution, which relies on imaging in regions with thinner ice. Employing an imaging strategy that is unlikely to capture eIF3-containing states

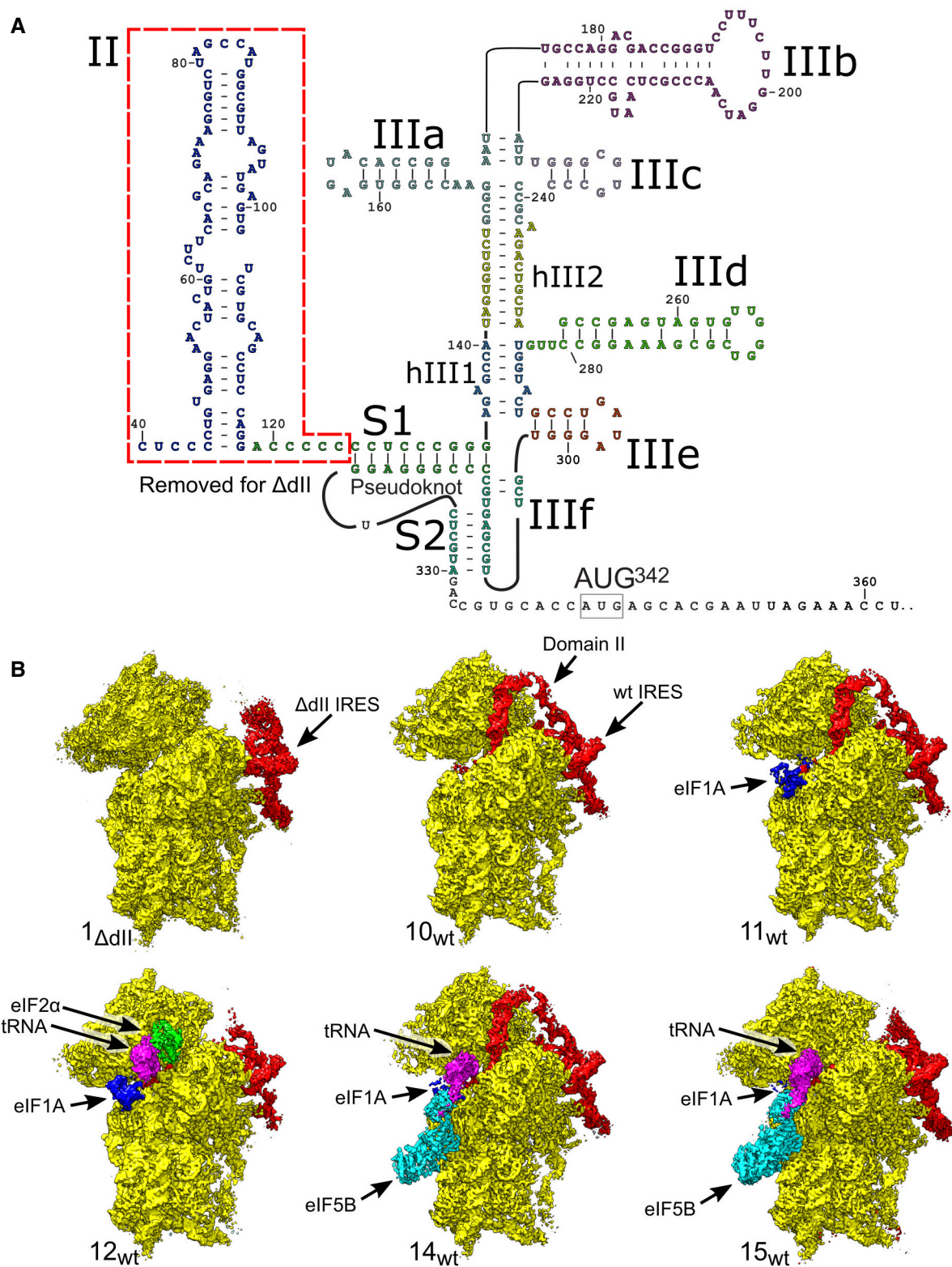


**Figure 1. Overview of HCV IRES-mediated initiation complexes.**

A Secondary structure of the HCV IRES, annotated to show individual elements.

B Segmented maps of the indicated ribosomal complexes assembled on the *wt* or  $\Delta$ dII HCV IRES, showing the 40S subunit (yellow), IRES (red), eIF1A (blue), Met-tRNA<sup>Met</sup> (magenta), and initiation factors eIF2 (green) or eIF5B (cyan).

does not affect data interpretation because all complexes studied can be assembled efficiently without eIF3 (Pestova *et al*, 1998b, 2008) and because the structure of the IRES is not affected by the binding of eIF3 (Sizova *et al*, 1998).

The structures obtained comprise the 40S/IRES<sub>ΔdII</sub> binary complex in various conformational states (structures 1<sub>ΔdII</sub>-9<sub>ΔdII</sub>); the 40S/IRES<sub>wt</sub> binary complex in a single conformational state (structure 10<sub>wt</sub>); the 40S/eIF1A/IRES<sub>wt</sub> ternary complex (structure 11<sub>wt</sub>); 48S ICs containing 40S subunits in the closed conformation, eIF2, Met-tRNA<sub>i</sub><sup>Met</sup>, eIF1A, and the *wt* or the ΔdII IRES (structures 12<sub>wt</sub> and 12<sub>ΔdII</sub>); 48S complexes containing the *wt* or the ΔdII IRES base-paired with the P-site Met-tRNA<sub>i</sub><sup>Met</sup> but lacking eIF2 and thus likely mimicking the stage after eIF2 dissociation following hydrolysis of GTP (structures 13<sub>wt</sub> and 13<sub>ΔdII</sub>); the pre-48S IC containing 40S subunits in the open conformation, eIF5B, eIF1A, and the *wt* IRES base-paired with P-site Met-tRNA<sub>i</sub><sup>Met</sup> and IRES dII inserted into the E site (structure 14<sub>wt</sub>); and 48S ICs containing 40S subunits in the closed conformation, eIF5B, eIF1A, Met-tRNA<sub>i</sub><sup>Met</sup>, and the *wt* or the ΔdII IRES (structures 15<sub>wt</sub> and 15<sub>ΔdII</sub>; Figs 1B and EV1A).

Thus, the structures obtained cover the entire initiation pathway, from the initial binding of the IRES to the 40S subunit to the formation of the eIF5B-containing 48S complex prior to subunit joining.

### Stepwise binding of the IRES to the 40S subunit

All previously published structures of the IRES showed domains IIIa/IIIc/IIId/IIIe/IIIf in an identical conformation on the platform side of the 40S subunit, regardless of the presence or absence of domain II (Spahn *et al*, 2001; Quade *et al*, 2015; Yamamoto *et al*, 2015; Weisser *et al*, 2017; Yokoyama *et al*, 2019). Although domain II is required for efficient translation (e.g. Reynolds *et al*, 1996; Filbin & Kieft, 2011) its contribution to IRES binding to the ribosome is minor and binding occurs with similar affinity for both the *wt* and ΔdII IRES (Kieft *et al*, 2001; Ji *et al*, 2004). For both *wt* and ΔdII IRES, their structures show binding to the 40S subunit platform involves multiple contacts formed by regions of the IRES (domains IIIa, IIIc, IIId, IIIe, and helix (h) S2) and ribosomal proteins eS1, eS27, and eS28, and h26 in ES7 of 18S rRNA (e.g., Quade *et al*, 2015; Weisser *et al*, 2017; Yamamoto *et al*, 2015; Fig EV1B). Deletion or mutation of these domains (IIIa-f) impairs ribosomal binding of the IRES to different extents, reflecting their cumulative importance (Kieft *et al*, 2001; Ji *et al*, 2004). In contrast to all previous structures of the HCV IRES, we observed a small proportion of 40S/IRES binary complexes formed on the ΔdII IRES with conformational differences in the individual positions of domains IIIa/IIIc/IIId/IIIe/IIIf (structures 1<sub>ΔdII</sub>-6<sub>ΔdII</sub>). Examination of these complexes (structures 1<sub>ΔdII</sub>-5<sub>ΔdII</sub>) revealed the ΔdII IRES undergoing a transition from a minimally associated state (structure 1<sub>ΔdII</sub>) to the canonically bound conformation observed here (structures 6<sub>ΔdII</sub> and 7<sub>ΔdII</sub>-15<sub>wt/ΔdII</sub>) and elsewhere (e.g., Spahn *et al*, 2001; Quade *et al*, 2015; Yamamoto *et al*, 2015; Weisser *et al*, 2017; Yokoyama *et al*, 2019). By ordering structures 1<sub>ΔdII</sub>-6<sub>ΔdII</sub> based on the number of IRES-40S subunit contacts we inferred a putative sequence of binding events between the ΔdII IRES and the 40S subunit (Fig 2A and Appendix Table S4).

Comparison between the least- and the most-bound states (structures 1<sub>ΔdII</sub> and 6<sub>ΔdII</sub>) shows that the IRES domains undergo displacement of varying extents during IRES binding (Fig 2B). Across all

structures, the most uniform regions of the IRES are the linked domains IIIa and IIIc (Fig 2A and B), which are known to contact eS27 via nt. 163 and 233 (Quade *et al*, 2015; Yamamoto *et al*, 2015). Given that we identified no complexes in which domain IIIa/IIIc showed major conformational differences regardless of the conformation of the rest of the IRES, the impairment of IRES activity by nucleotide substitutions in these domains (e.g., Tang *et al*, 1999; Kieft *et al*, 2001), suggests that the observed interactions between domain IIIa/IIIc and eS27 are critical for correct IRES binding to the 40S subunit and hence for function. Other IRES domains are more dynamic. Thus, to transition from the least- to the most-bound states involves the translation of domain IIIId by 10.6 Å toward the intersubunit face and domains hIII<sub>1</sub>/IIIe/III<sub>f</sub> by 23.3 Å toward the mRNA exit channel, whereas domains IIIa/IIIc move by 5.9 Å (Fig 2B). The relative differences in the displacement of these domains show how the IRES attaches to the ribosome in a zipper-like fashion by building consecutive contacts from the stable domain IIIa/IIIc region to the terminal domains hIII<sub>1</sub>/IIIe/III<sub>f</sub>.

The local resolution was sufficient to identify specific 40S/IRES contacts and to follow their dynamics in structures 1<sub>ΔdII</sub>-6<sub>ΔdII</sub>. The IRES fully bound to 80S ribosomes form six interactions with ES7: four Watson-Crick base pairs between ES7 nt. U<sub>1115</sub> and C<sub>1116-1118</sub> and IRES domains hIII<sub>1</sub> (A<sub>136</sub>) and IIIId (GGG<sub>266-268</sub>), respectively; a reverse Hoogsteen base pair between ES7 nt. U<sub>1114</sub> and domain IIIe (A<sub>296</sub>); and a stacking interaction between ES7 nt. U<sub>1114</sub> and domain IIIe (G<sub>295</sub>; Quade *et al*, 2015; Yamamoto *et al*, 2015). Although this network of interactions is present in structures 6<sub>ΔdII</sub> and 7<sub>ΔdII</sub>-15<sub>wt/ΔdII</sub>, the full complement was not observed during the early-stage association of the IRES with the 40S subunit (structures 1<sub>ΔdII</sub>-5<sub>ΔdII</sub>; Fig 2B and Appendix Table S4). Initially, structure 1<sub>ΔdII</sub> showed only two of the six canonical interactions with ES7, namely the base pairs between domain IIIId (G<sub>267-268</sub>) and ES7 nt. C<sub>1116-1117</sub>. The position of domain IIIId in structure 1<sub>ΔdII</sub> also allows some interaction between this domain and α-helix 6 in eS1, a region that contains Lys199, a residue that interacts with domain IIIe in the fully bound IRES (Quade *et al*, 2015; Yamamoto *et al*, 2015). These contacts between ES7 and domain IIIId, along with the domain IIIa/IIIc interactions with eS27 are the only bonds between the IRES and the 40S subunit in this complex. Structure 2<sub>ΔdII</sub> maintains all of these contacts, but the repositioning of domain IIIId by 4.4 Å relative to structure 1<sub>ΔdII</sub> allows for the formation of the third Watson-Crick base pair, between ES7 (C<sub>1118</sub>) and domain IIIId (G<sub>266</sub>). In the following complex (structure 3<sub>ΔdII</sub>), domain IIIId moves closer to the 40S platform by 2.8 Å; hS1/hS2/hIII<sub>1</sub>/IIIe/III<sub>f</sub> moves by 5.0 Å, whereas the position of the stable domain IIIa/IIIc changes by only 1.5 Å. This repositioning breaks none of the contacts observed in structure 2<sub>ΔdII</sub> and allows the formation of a stacking interaction between domain IIIe G<sub>295</sub> and ES7 U<sub>1114</sub>. The subsequent complex, structure 4<sub>ΔdII</sub>, maintains all previous contacts and forms the fifth interaction with ES7, between domain IIIe (A<sub>296</sub>) and ES7 (U<sub>1114</sub>). Globally, the IRES domains continue to move closer to their canonically bound positions, with domain IIIId shifting by 2.8 Å and domains hS1/hIII<sub>1</sub>/IIIe/III<sub>f</sub> moving by 4.7 Å compared with structure 3<sub>ΔdII</sub>. Although structures 5<sub>ΔdII</sub> and 6<sub>ΔdII</sub> have both formed the final canonical contact, a base pair between domain hIII<sub>1</sub> (A<sub>136</sub>) and ES7 (U<sub>1115</sub>), these complexes differ by the position of hS1 and the degree of accommodation of hS2/III<sub>f</sub>, with structure 6<sub>ΔdII</sub> resembling the fully accommodated state (e.g., structures 7<sub>ΔdII</sub>-15<sub>wt/ΔdII</sub>). Structures

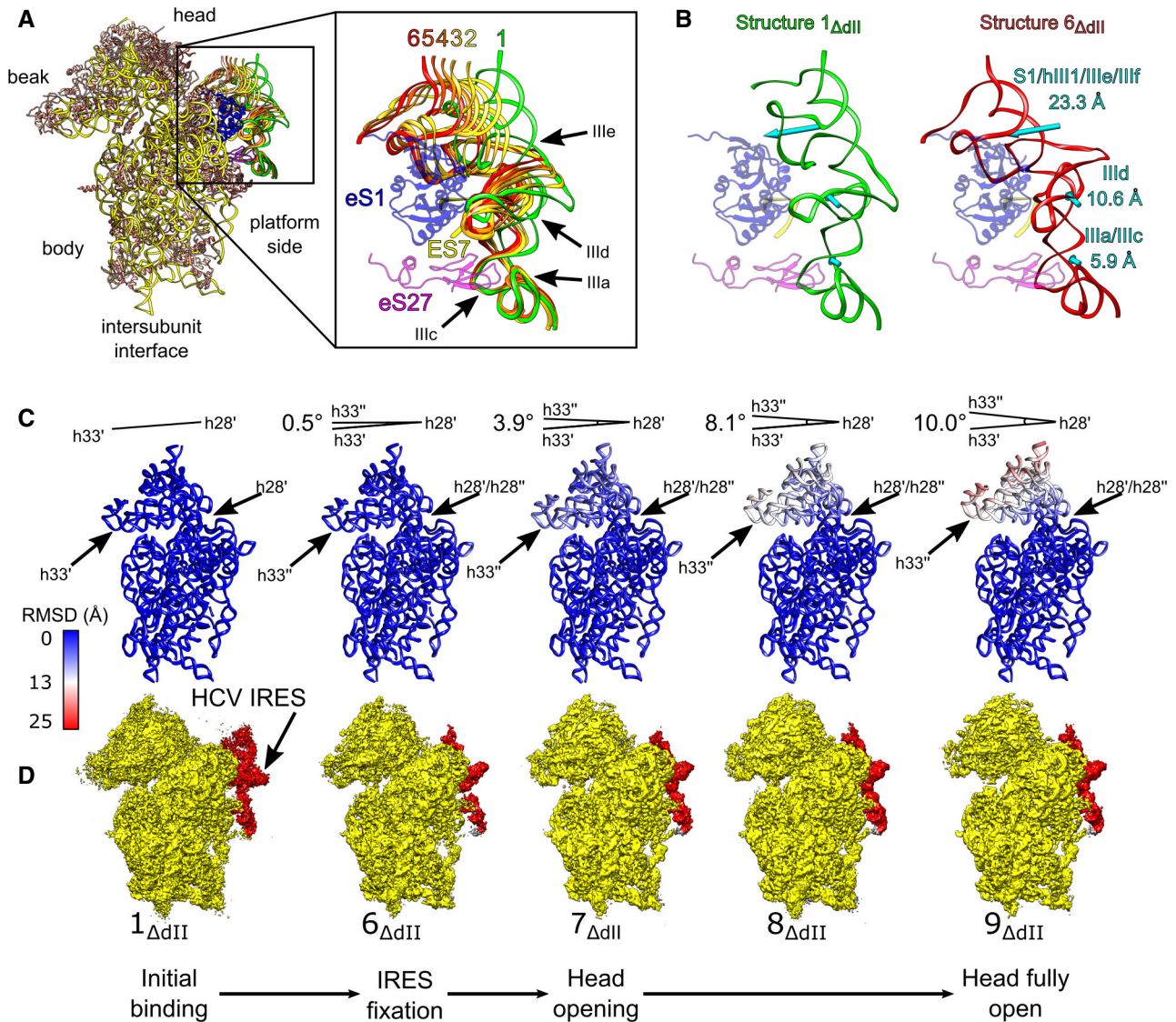


**Figure 2. Initial events during binding of the HCV IRES to the 40S subunit.**

- A IRES models from structures 1 $\Delta$ dII–6 $\Delta$ dII aligned on the 40S subunit. IRES domains and ribosomal proteins eS1 (blue), eS27 (magenta), and 18S rRNA ES7 (yellow) are indicated (inset).
- B Comparison between minimally bound (structure 1 $\Delta$ dII) and fully bound (structure 6 $\Delta$ dII) IRES complexes showing the displacement of the indicated IRES domains (cyan arrows).
- C RMSD (Å) of 18S rRNA for complexes shown directly underneath in (D) relative to the minimally bound state (structure 1 $\Delta$ dII), color-coded as in the inset key. The angle formed between helix 33 (h33') and helix 28 (h28') in structure 1 $\Delta$ dII and helix 33 (h33'') in other complexes is indicated.
- D Segmented maps for the indicated complexes showing the 40S subunit (yellow) and IRES (red) organized in a putative sequence showing the minimally bound state (structure 1 $\Delta$ dII), canonical IRES binding (structure 6 $\Delta$ dII), and the induction of opening of the head of the 40S subunit (structures 7 $\Delta$ dII–9 $\Delta$ dII).

5 $\Delta$ dII and 6 $\Delta$ dII are also the first complexes in which the IRES is in a position to form a hydrogen bond between Asn147 in eS1 and the phosphate backbone of GG<sub>300–301</sub>, an interaction that is maintained in all subsequent complexes.

Taken together, this series of structures (1 $\Delta$ dII–6 $\Delta$ dII) indicates that domains IIIa/IIIc, the first elements of the IRES to form canonical contacts with the 40S subunit, act as a pivot to complete the docking of domain IIIc and hIII1/IIIe/IIIb onto ES7. These structures (1 $\Delta$ dII–6 $\Delta$ dII) may potentially represent transient states in the binding of

both the  $\Delta$ dII and *wt* IRES, which we were able to capture in samples prepared using the  $\Delta$ dII IRES because the altered kinetic landscape of the initiation pathway in the absence of domain II allowed them to accumulate.

An important corollary of IRES binding is the conformational changes that occur in the 40S subunit. Whereas complexes with an incompletely accommodated IRES (structures 1 $\Delta$ dII–5 $\Delta$ dII) contain 40S subunits in the same closed conformation, ribosomal structures with the full complement of IRES/40S contacts (structure 6 $\Delta$ dII–9 $\Delta$ dII)

show striking differences in the position of the head, from the closed conformation in structure 6 $_{\Delta\text{dII}}$  (matching the head position in structures 1 $_{\Delta\text{dII-5}\Delta\text{dII}}$ ) to the fully open state in structure 9 $_{\Delta\text{dII}}$  (Fig 2C and D). Although structures 7 $_{\Delta\text{dII-9}\Delta\text{dII}}$  have a canonically bound IRES with domain III contacting eS1, eS27, and ES7 as in structure 6 $_{\Delta\text{dII}}$ , they show large-scale conformational changes to the head as the 40S subunit transitions from semi-closed (structure 7 $_{\Delta\text{dII}}$ ) to fully open (structure 9 $_{\Delta\text{dII}}$ ) states. Thus, structure 7 $_{\Delta\text{dII}}$  opens by 3.9°, structure 8 $_{\Delta\text{dII}}$  by 8.1°, and structure 9 $_{\Delta\text{dII}}$  by 10.0° compared with the conformation of the 18S rRNA in structures 1 $_{\Delta\text{dII-6}\Delta\text{dII}}$ . These global changes to the position of the 40S head are reflected in changes in the P site as the distance between U<sub>1248</sub> and C<sub>1701</sub> increases from 7.3 Å, to 9.9 Å and finally to 11 Å in structures 7 $_{\Delta\text{dII}}$ , 8 $_{\Delta\text{dII}}$ , and 9 $_{\Delta\text{dII}}$ , respectively.

Thus, even in the absence of domain II, the establishment of the full complement of IRES/40S contacts results in the transition of the 40S subunit from the closed to the open state, which is required for the accommodation of the initiation codon and surrounding regions in the mRNA-binding channel.

#### Accommodation of the IRES in the mRNA-binding channel

In contrast to 40S/IRES binary complexes assembled on the  $\Delta\text{dII}$  IRES, which showed differences in the conformation of the 40S subunit head and IRES position, binary complexes assembled on the *wt* IRES yielded a uniform structure that was refined to 3.8 Å resolution from 119,320 particles (structure 10 $_{\text{wt}}$ ; Fig 1B). Both the conformation of the 40S subunit and its contacts with IRES domains IIIa/IIIc/IIIe/IIIe/IIIe in structure 10 $_{\text{wt}}$  are identical to those in structure 9 $_{\Delta\text{dII}}$  (Fig EV2A and B). Structure 10 $_{\text{wt}}$  was assembled using the *wt* IRES, and so, domain II is present and inserted into the 40S subunit E site, in a conformation identical to that observed in IRES/80S complexes (Quade *et al.*, 2015; Yamamoto *et al.*, 2015). Superposition of structure 10 $_{\text{wt}}$  and a closed-state 40S subunit shows that in the latter, steric clashes between uS7 and domain II would prohibit insertion of this domain into the E site. Thus, domain II prevents the 40S subunit from returning to the closed state.

For the *wt* IRES, we also obtained the structure of the 40S-IRES-eIF1A ternary complex that was refined to 3.8 Å resolution from 204,782 particles (structure 11 $_{\text{wt}}$ ; Fig 1B). The conformation of the 40S subunit and the position of the IRES were identical to those in the 40S/IRES $_{\text{wt}}$  binary complex (structure 10 $_{\text{wt}}$ ; Figs 1B and EV2B). The complex clearly shows density for eIF1A located between 18S rRNA h44 and the ribosomal proteins eS30 and uS12, allowing us to model the OB domain and the C-terminal subdomain of eIF1A (residues 22–122). Although structure 11 $_{\text{wt}}$  lacks tRNA and the 40S subunit is in the open state, the position and conformation of eIF1A on the ribosome are identical to those in canonical 48S complexes (Brito Querido *et al.*, 2020; Simonetti *et al.*, 2020).

As expected, binary complexes assembled on the  $\Delta\text{dII}$  IRES and containing the 40S subunit in the closed conformation (1 $_{\Delta\text{dII-6}\Delta\text{dII}}$ ) do not have mRNA in the mRNA-binding channel. However, although structures 9 $_{\Delta\text{dII}}$ , 10 $_{\text{wt}}$ , and 11 $_{\text{wt}}$  all have 40S subunits in the identical open conformation that is required for loading mRNA into the channel, they differ strongly in the degree of accommodation of the initiation codon and surrounding regions (Fig EV2A and B). In the 40S/IRES $_{\Delta\text{dII}}$  binary complex (structure 9 $_{\Delta\text{dII}}$ ) there is clear density for mRNA only in the exit portion of the channel up to the (–8)

position (HCV nt 334; Fig 3A). The *wt* 40S/IRES binary complex (structure 10 $_{\text{wt}}$ ), on the other hand, shows density corresponding to mRNA from the exit portion, through the E site, where it is stabilized by domain II, to AU<sub>342-3</sub> in the P site (Fig 3B). The (+3) nucleotide, G<sub>344</sub>, could not be identified due to disorder in the map. Although there is additional mRNA density in the mRNA channel ~8 Å from the (+3) P-site nucleotide, the identity of these nucleotides does not correspond to those that immediately follow the start codon, and this density extends 20 Å out from the mRNA channel, suggesting that after the P site, the mRNA is looped out. Thus, the presence of domain II results in accommodation of the additional nine nucleotides from the mRNA exit to the P site (i.e., from G<sub>335</sub> to U<sub>343</sub>), while density corresponding to mRNA located downstream from the P site is likely a mixture of different sequence registers of mRNA. Strikingly, the presence of eIF1A in ribosomal complexes (structure 11 $_{\text{wt}}$ ) resulted in the accommodation of mRNA along the entire mRNA-binding cleft (Fig 3C). Examination of critical P-site nucleotides for all complexes shows that in each case C<sub>1701</sub> of 18S rRNA is in a single conformation, except for the binary complex prepared with the *wt* IRES (structure 10 $_{\text{wt}}$ ), where it is present in two states as determined by examination of the Coulomb potential around that nucleotide (Fig 3D). In the conformation of the second state, C<sub>1701</sub> contacts the upstream mRNA base U<sub>343</sub>(+2), possibly contributing to stabilizing the mRNA when it has not been completely accommodated in the mRNA channel at the P site. The highly conserved C<sub>1698</sub> (Prince *et al.*, 1982) contacts downstream mRNA and may act as a sensor to stimulate C<sub>1701</sub> adopting the second conformation in which it can stabilize the incompletely loaded mRNA.

Taken together, the structures of binary complexes assembled on  $\Delta\text{dII}$  and *wt* IRESs, and the eIF1A-containing complex assembled on the *wt* IRES provide structural insight into the roles of domain II and eIF1A in sequentially loading the mRNA channel. Even though the  $\Delta\text{dII}$  IRES induces the open conformation of the 40S subunit that is required for the accommodation of mRNA in the mRNA-binding channel, accommodation in this case is only partial, and the 40S subunit is not stably present in the open conformation. This is consistent, on one hand, with the ability of the  $\Delta\text{dII}$  IRES to function in initiation, but also, on the other hand, with it being less active than the *wt* IRES (e.g., Reynolds *et al.*, 1996). The presence of domain II results in accommodation of the initiation codon and the upstream region in the mRNA-binding channel, thereby enhancing the efficiency of initiation (Reynolds *et al.*, 1996), whereas eIF1A promotes mRNA fixation downstream from the P site, accounting for its stimulatory role (Jaafar *et al.*, 2016).

#### The structure of eIF2-containing 48S complexes assembled on the HCV IRES

The structures of eIF2-containing 48S ICs assembled on the *wt* and  $\Delta\text{dII}$  IRES were refined from 46,904 and 103,813 particles to resolutions of 3.6 and 3.5 Å, respectively (structures 12 $_{\text{wt}}$  and 12 $_{\Delta\text{dII}}$ ; Figs 1B and EV1A, and Appendix Fig S1). Both *wt* and  $\Delta\text{dII}$  IRES 48S ICs form identical complexes with respect to the 40S subunit's closed conformation, the positions of Met-tRNA<sup>Met</sup>, eIF2, and eIF1A, and the established P-site codon-anticodon base pairing (Figs 1B, and EV3A and B). The IRES-containing 48S IC is also structurally identical to the canonical 48S complex formed by cap-

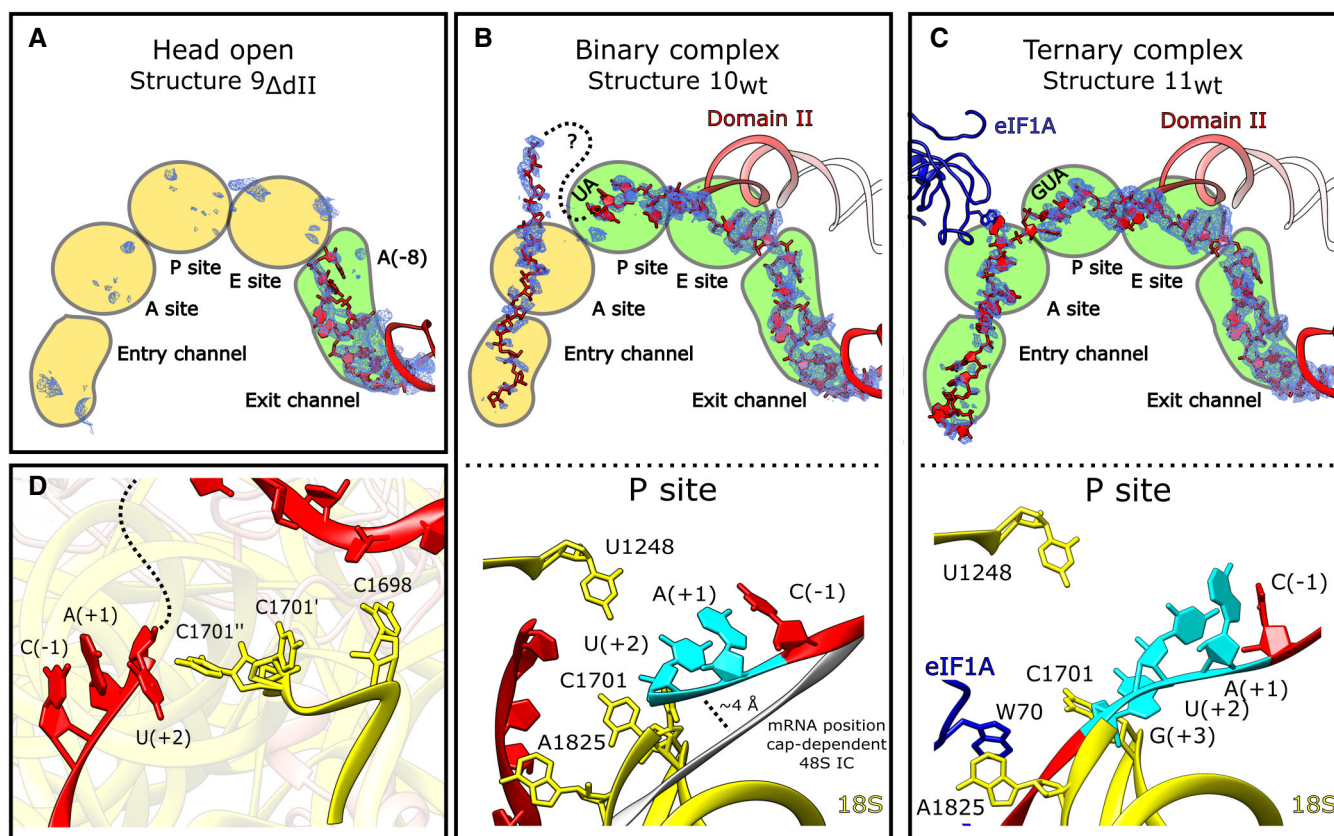


**Figure 3. The roles of IRES domain II and eIF1A in loading mRNA into the mRNA channel.**

A–D (A and upper panels of B and C) The mRNA channel spanning the entry and exit channels, A, P, and E sites viewed through the ribosome head toward the body for the indicated complexes. The IRES (red), Coulomb potential (blue mesh), and eIF1A (blue) are shown. (Lower panels of B and C) P site showing mRNA interactions for the (B) binary complex (structure 10<sub>wt</sub>) and the (C) eIF1A-containing ternary complex (structure 11<sub>wt</sub>). 18S rRNA (yellow), eIF1A (blue), IRES mRNA (red) with start codon (cyan) are all marked. (B) The position of mRNA modeled in the canonical cap-dependent 48S IC (PDB: 6ZMW) is shown in gray. (D) Position of key nucleotides in the P site in structure 10<sub>wt</sub> showing interactions between incompletely loaded mRNA and C<sub>1698</sub> resulting in C<sub>1701</sub> sampling dual conformations near the (+2) position.

dependent initiation (e.g., Simonetti *et al*, 2020) with respect to the global conformation of the 40S subunit and the placement of Met-tRNA<sub>i</sub><sup>Met</sup>, eIF2 $\alpha$ , and eIF1A. Thus, the E site-associated eIF2 $\alpha$  contacts the highly conserved uS7/Asp194 directly and interacts with Met-tRNA<sub>i</sub><sup>Met</sup> via Thr103, Arg67, and His114 (Fig 4A). As with canonical 48S ICs (Hussain *et al*, 2014; Simonetti *et al*, 2020), eIF2 $\alpha$  forms hydrogen bonds with the (–3) adenosine via Arg55, a contact that enhances codon selection in the scanning mode of initiation, presumably by stabilizing the arrested 48S IC (Pisarev *et al*, 2006; Thakur *et al*, 2020). Contacts between eIF2 $\alpha$  Arg57 and the tRNA acceptor stem loop (ASL) and the 18S rRNA that occur in canonical 48S ICs (Simonetti *et al*, 2020) are also present (Fig 4A). The unsharpened map also contained density corresponding to eIF2 $\gamma$  (Fig 4B) identical to that seen in cap-dependent 48S ICs (Simonetti *et al*, 2020), but it had a low local resolution at the acceptor end of Met-tRNA<sub>i</sub><sup>Met</sup> and was not modeled after map sharpening. The occupancy of the mRNA-binding channel for 48S ICs prepared on both *wt* and  $\Delta$ dII IRESs (Structures 12<sub>wt/ $\Delta$ dII</sub>) is identical, with mRNA density present from the exit channel through the E, P, and A sites to the entry region. The observation that eIF2 $\alpha$  interacts via Arg55 with the (–3) context nucleotide, as in the canonical initiation

process, is consistent with its importance in HCV IRES function (Ma *et al*, 2018).

The position of domain II differs substantially between the 48S IC and the corresponding 40S/IRES binary and 40S/eIF1A/IRES ternary complexes assembled on the *wt* IRES (structures 12<sub>wt</sub>, 10<sub>wt</sub>, and 11<sub>wt</sub>, respectively). In both the binary and ternary complexes, it is inserted into the E site, a position that is incompatible with the binding of eIF2. Thus, in the 48S IC, domain II is oriented away from the subunit interface, toward the solvent side of the 40S subunit, and shows an attenuation of density so that a model of domain II is not fully enclosed by the map. Focused classification of this region revealed that domain II is flexible and occupies multiple conformations oriented away from the E site (Fig 4C and Appendix Table S5). Interestingly, eIF2 $\alpha$  Arg55 contacting the mRNA at A(–3) in 48S ICs is in the same position as C<sub>83</sub> in IRES domain II in the 40S/eIF1A/IRES ternary complex, indicating that this location in the E site is important for stabilizing the mRNA regardless of the conformation of the 40S subunit and of differences in the position of mRNA at other locations along the mRNA-binding channel.

Compared with the open binary or ternary complexes (structures 10<sub>wt</sub> and 11<sub>wt</sub>), the head of the 40S subunit in 48S ICs formed on

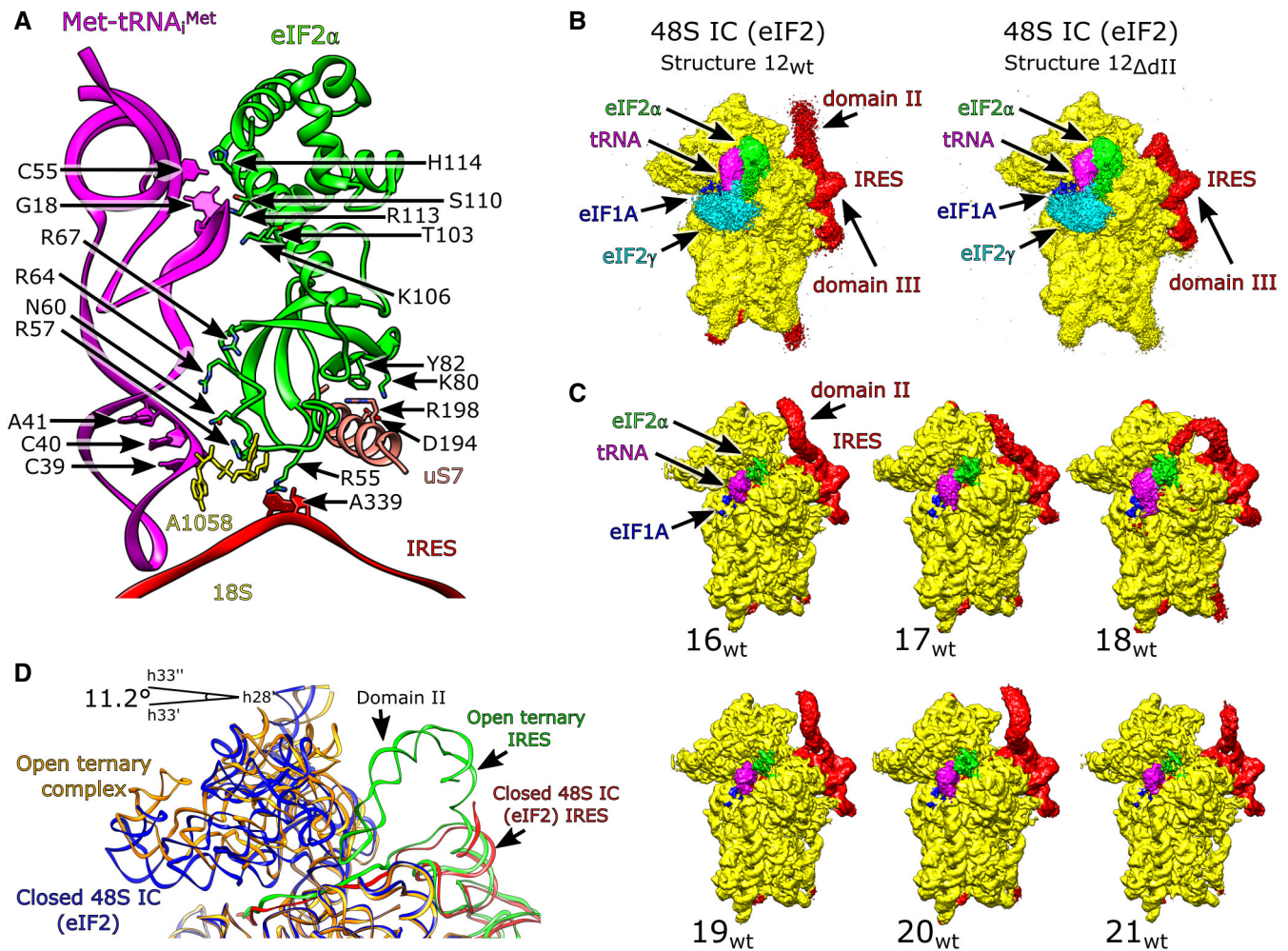


**Figure 4. The HCV IRES-eIF2-containing 48S initiation complex.**

- A Contacts between eIF2 $\alpha$  and the HCV IRES, Met-tRNA<sup>Met</sup>, and the 40S subunit.  
 B Unsharpened maps for 48S ICs formed on the wt IRES (structure 12<sub>wt</sub>), left, and the  $\Delta$ dII IRES (structure 12 <sub>$\Delta$ dII</sub>), right. Comparison with canonical cap-dependent initiation complexes (PDB: 6YAL) identifies the presence of eIF2 $\gamma$  (cyan).  
 C IRES domain II occupies multiple positions in 48S ICs formed on the wt IRES.  
 D Conformation of 18S rRNA in the open ternary complex (structure 11<sub>wt</sub>) and the eIF2-containing 48S IC (structure 12<sub>wt</sub>).

both wt and  $\Delta$ dII IRESs is in a closed position, having moved by 11.2° relative to the open states (Fig 4D). This position is in an even more closed conformation than in closed binary complexes (structures 1 <sub>$\Delta$ dII-6 $\Delta$ dII</sub>), in which the position of the head differed from that in structures 10<sub>wt</sub> and 11<sub>wt</sub> by  $\sim$ 9.0° (Fig EV2B). This indicates that the formation of the codon-anticodon interaction, seen in structures 12<sub>wt/ $\Delta$ dII</sub>, causes the ribosome to enter a distinct closed conformation matching that is observed for both yeast and mammalian canonical cap-dependent 48S ICs (e.g., Ll acer *et al*, 2015; Simonetti *et al*, 2020). This closed state likely serves as a signal that an appropriate start codon has been identified so that subsequent initiation steps can proceed (Ogle *et al*, 2002).

We also obtained 40S complexes containing platform-bound wt or  $\Delta$ dII IRES and P-site Met-tRNA<sup>Met</sup> but lacking all initiation factors (structures 13<sub>wt</sub> and 13 <sub>$\Delta$ dII</sub>; Fig EV1A). These closed complexes, refined from 15,906 and 15,598 particles to 4.6 and 4.4  , respectively, showed clear density for codon-anticodon base pairing

(Appendix Fig S3G and Table S3). It is unclear whether initiation factors dissociated due to slow eIF5-independent hydrolysis of eIF2-bound GTP (Unbehauen *et al*, 2004), or through denaturation at the air-water interface and/or due to the shear forces associated with blotting (d'Imprima *et al*, 2019; Glaeser, 2021). In any case, this complex likely mimics an intermediate state immediately after eIF2 dissociation and prior to the binding of eIF5B.

#### The structure of eIF5B-containing 48S complexes assembled on the IRES

Classification of eIF5B-containing ribosomal complexes yielded two structures formed on the wt IRES (structures 14<sub>wt</sub> and 15<sub>wt</sub>) and one structure (15 <sub>$\Delta$ dII</sub>) assembled on the  $\Delta$ dII IRES, which were refined to 3.8, 3.7, and 3.7   resolution from 60,578, 133,782, and 61,648 particles, respectively (Figs 1B and EV1A). All structures contain eIF5B, eIF1A, and the P-site Met-tRNA<sup>Met</sup> base-paired with the initiation



codon. Structures 15<sub>wt</sub> and 15<sub>ΔdII</sub> were in the same closed conformation (Fig EV4A and B, and Appendix Fig S4A), identical to that in 48S ICs assembled on canonical cap-dependent mRNA (Simonetti *et al*, 2020), and were accordingly classified as 48S ICs. Thus, in eIF5B- and eIF2-containing 48S ICs, 18S rRNA nucleotides C<sub>1701</sub> and U<sub>1248</sub> are separated by ~3.5 Å, and the contacts of the P-gate nucleotides G<sub>1639</sub> and A<sub>1640</sub> in the 18S rRNA and Arg146 in uS9, with the tRNA anticodon arm on the opposite side to the anticodon, are also present in both 48S ICs. Similar to eIF2-containing 48S ICs, in eIF5B-containing ICs assembled on the *wt* IRES (structure 15<sub>wt</sub>), domain II is oriented away from the subunit interface, toward the solvent side of the 40S subunit, and shows an attenuation of density so that the model of domain II is not fully enclosed by the map. Focused classification of this region revealed that domain II is flexible and occupies multiple conformations oriented away from the E site (Appendix Fig S4B and Table S5).

However, in contrast to structures 15<sub>wt/ΔdII</sub>, the 40S subunit in structure 14<sub>wt</sub> is in an open conformation with domain II inserted into the E site, which led us to designate this structure as pre-48S IC (Fig 1B). In the eIF5B-containing pre-48S IC, the separation between C<sub>1701</sub> and U<sub>1248</sub> is increased to ~11 Å, and tRNA does not contact the P gate or uS9. In all structures, eIF1A occupies its usual position over h44 and eS30 and uS12, whereas eIF5B resides on the intersubunit face of the 40S subunit as in 80S ribosomal complexes (Yamamoto *et al*, 2014; Huang & Fernández, 2020; Wang *et al*, 2020). Both eIF5B-containing pre-48S ICs (structure 14<sub>wt</sub>) and 48S ICs (structure 15<sub>wt/ΔdII</sub>) showed full occupancy of the entire mRNA-binding channel, from the exit portion through the E, P, and A sites to the entry region.

All structures show clear density for eIF5B residues 592–1,218, corresponding to all major domains (Fig EV4C). This is the first high-resolution structure of mammalian eIF5B and also the first structure of the 40S/eIF5B subunit complex prior to subunit joining. Although we used full-length native eIF5B, extensive 3D classification and processing did not reveal any structure corresponding to the N-terminal region, suggesting that it is highly disordered, an observation that is supported by the structure of full-length eIF5B predicted using AlphaFold (Jumper *et al*, 2021). In all structures, the G domain and domains II and III form the central core of eIF5B that connects via domain III and helix 12 to the tRNA acceptor stem-binding domain IV (Fig EV4C). All complexes also contained eIF5B-bound GTP (Appendix Fig S4C), and consistently, showed switch 1, switch 2, and the β9-β10 loop in domain II in the GTP-bound conformation, identical to that in fungal GTP-bound eIF5B (Kuhle & Ficner, 2014; Appendix Fig S4D).

We identified multiple contacts between eIF5B domains II and III and 18S rRNA h5, h14, and h15, and an interaction between eIF5B domain II and uS12 (Fig EV4C and Appendix Table S6) and noted that the β13-β14 loop (Appendix Fig S4E, green) could interfere with the transition of switch 1 from GTP-bound to GDP-bound (Appendix Fig S4E, blue and cyan). However, on the yeast 80S ribosome, the β13-β14 loop of GTP-bound eIF5B contacts A<sub>415</sub> in 18S rRNA h14 and is positioned away from the path that switch 1 might take as it changes to the GDP-bound conformation (Wang *et al*, 2020; Appendix Fig S4E, red). Although there is no contact between the equivalent nucleotide (A<sub>464</sub>) and β13-β14 in our complexes, h14 is accessible. These observations suggest that the 60S subunit might stimulate the interaction between A<sub>415</sub> and the β13-

β14 loop to reposition this loop away from switch 1 so that a transition from the GTP- to the GDP-bound conformation is possible. In both pre-48S ICs and 48S ICs, the position of domain IV also allows it to contact eIF1A via interactions between His112 in the helical subdomain of eIF1A (Battiste *et al*, 2000) and the extreme C-terminal region of eIF5B, and between the eIF1A L23 β-turn (near Gly54) and Arg1186 in domain IV of eIF5B (Fig 5A and B). These interactions are distinct from the previously reported binding of eIF1A's extreme C-terminal DDIDI sequence to the h12/h13 loop in eIF5B domain IV (Marintchev *et al*, 2003; Zheng *et al*, 2014) and of the eIF1A L45 loop to eIF5B domain III (Nag *et al*, 2016). Previously reported interactions involved isolated polypeptides and were detected by NMR (Marintchev *et al*, 2003; Nag *et al*, 2016) or X-ray crystallography (Zheng *et al*, 2014), whereas the interactions reported here were observed in functional 48S complexes.

Comparison of the position of the P-site Met-tRNA<sub>i</sub><sup>Met</sup> in the eIF2-containing 48S IC (Simonetti *et al*, 2020) and in the 80S ribosome (Yamamoto *et al*, 2014; Wang *et al*, 2020) shows that in the latter, tRNA has rotated 14° toward the 40S subunit body and the T-loop has moved by ~15 Å to allow placement of the acceptor stem into the P site of the 60S subunit. Comparison of eIF2- and eIF5B-containing 40S ribosomal complexes (structures 12<sub>wt/ΔdII</sub>, 14<sub>wt</sub>, and 15<sub>wt/ΔdII</sub>) revealed that in eIF5B-containing complexes, Met-tRNA<sub>i</sub><sup>Met</sup> has rotated by ~14° and has moved by 15 Å from the head of the 40S subunit to a position that matches the orientation seen in 80S structures (Wang *et al*, 2020; Fig 5A). This repositioning of tRNA was observed for all structures that contained eIF5B, indicating that eIF5B re-orientates Met-tRNA<sub>i</sub><sup>Met</sup> on the 40S subunit prior to subunit joining. However, despite the differences in the orientation of the acceptor arm of the P-site tRNA and the conformation of the 40S subunit, the anticodon loop in eIF2-containing 48S ICs, and eIF5B-containing 48S ICs and pre-48S ICs is positioned identically (Fig. 5A and B). Interestingly, although the overall position of eIF5B-Met-tRNA<sub>i</sub><sup>Met</sup> in eIF5B-containing 48S ICs and in 80S ribosomes is generally similar, upon binding of a 60S subunit, domain IV of eIF5B undergoes a 33° rotation toward the platform side of the 40S subunit, and a translation by 6.4 Å parallel to the mRNA channel toward the platform of the 40S subunit, which result in repositioning of the tRNA acceptor stem by 6.4 Å toward the ribosome head (i.e., toward ribosomal protein eS25) without changing the position of the ASL and with only minor movement of eIF5B helix 12 (Fig EV4D). Such repositioning of domain IV and the tRNA acceptor stem upon binding of a 60S subunit would avert steric clashes of domain IV with H84 of 28S rRNA and between uL16 and the tRNA acceptor stem (~A<sub>74</sub>; Fig EV4E). Similar repositioning of IF2 domain C2 (equivalent to eIF5B domain IV) to avoid analogous steric clashes was observed in bacteria upon joining of 50S subunits to 30S ICs (Hussain *et al*, 2016; Kaledhonkar *et al*, 2019). Adjustment of the orientation of initiator tRNA prior to subunit joining is a critical step in initiation, and the mechanism by which it is mediated, by rotation and translation of domain IV of the universally-conserved initiation factor IF2/eIF5B, likely appeared early in evolution.

#### Dynamics of ribosomal contacts of mRNA along the mRNA-binding channel throughout the initiation process

We next compared all complexes containing mRNA in the mRNA-binding channel (structures 9<sub>ΔdII</sub>-15<sub>wt/ΔdII</sub>) to determine how the

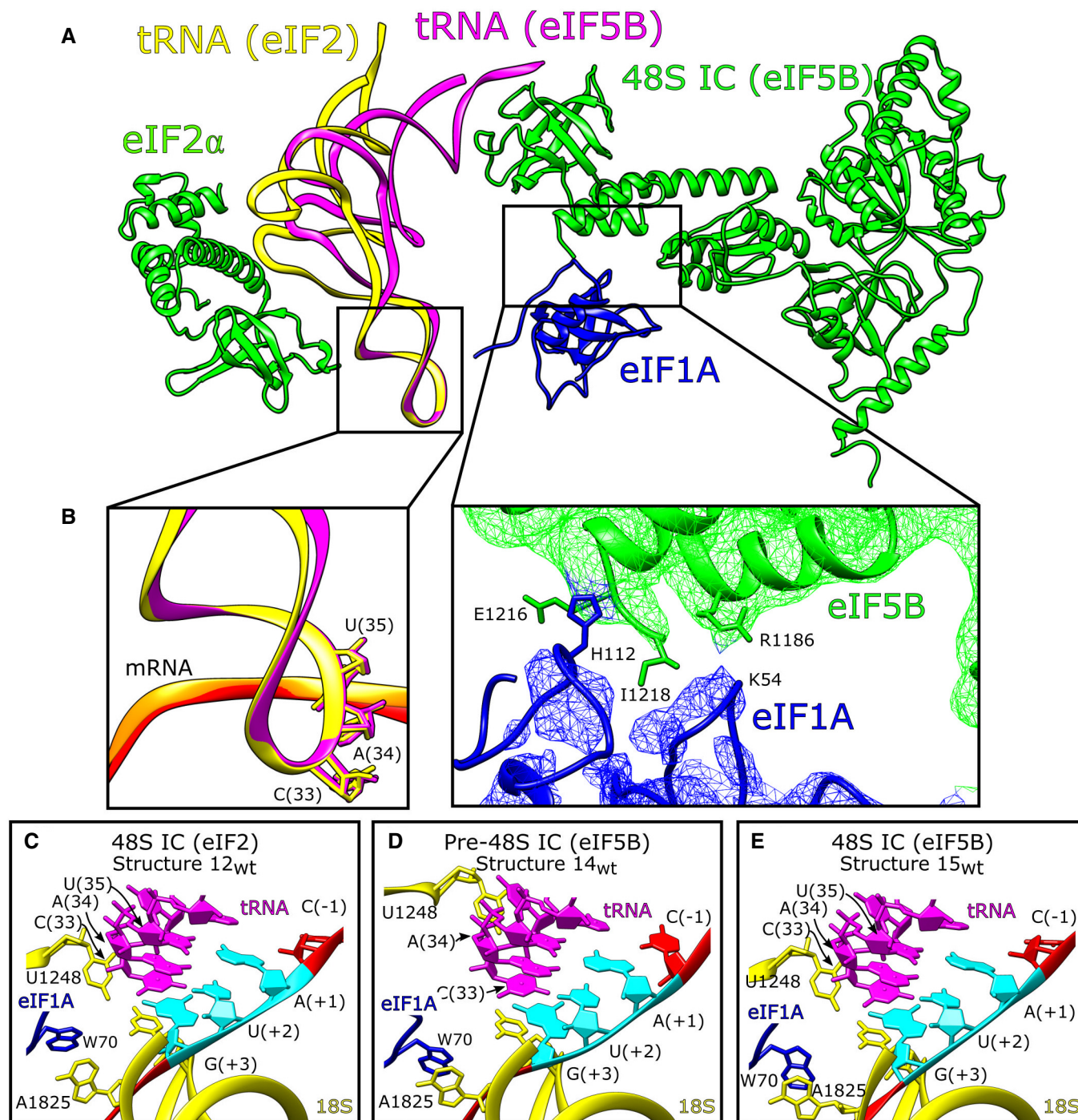


**Figure 5. The HCV IRES-eIF5B-containing 48S initiation complex.**

- A** Changes to the position of P site tRNA depending on the presence of either eIF2 or eIF5B. Upon binding of eIF5B, the T-arm, D-arm, and acceptor stem of Met-tRNA<sup>Met</sup> move by 15.6 Å and 14° relative to their positions in the eIF2-containing 48S complex.
- B** Inset showing the unchanged conformation of the tRNA acceptor stem loop in eIF2- and eIF5B-containing 48S complexes (left), and contacts between eIF5B domain IV and eIF1A (right).
- C–E** P site for (C) eIF2-containing 48S IC (structure 12<sub>wt</sub>), (D) eIF5B-containing pre-48S IC (structure 14<sub>wt</sub>), and (E) eIF5B-containing 48S IC (structure 15<sub>wt</sub>) showing 18S rRNA (yellow), Met-tRNA<sup>Met</sup> (magenta), eIF1A (blue), and IRES mRNA (red) with the start codon (cyan) marked.

conformational state of the 40S subunit and the presence of different translational components correlate with ribosomal interactions of defined mRNA regions along the channel and their consequent

stabilization (Fig 6A and B). The open-state binary 40S/IRES complexes (structures 9<sub>ΔdlI</sub> and 10<sub>wt</sub>) both show clear mRNA density at the exit portion of the mRNA-binding channel up to the (–8)

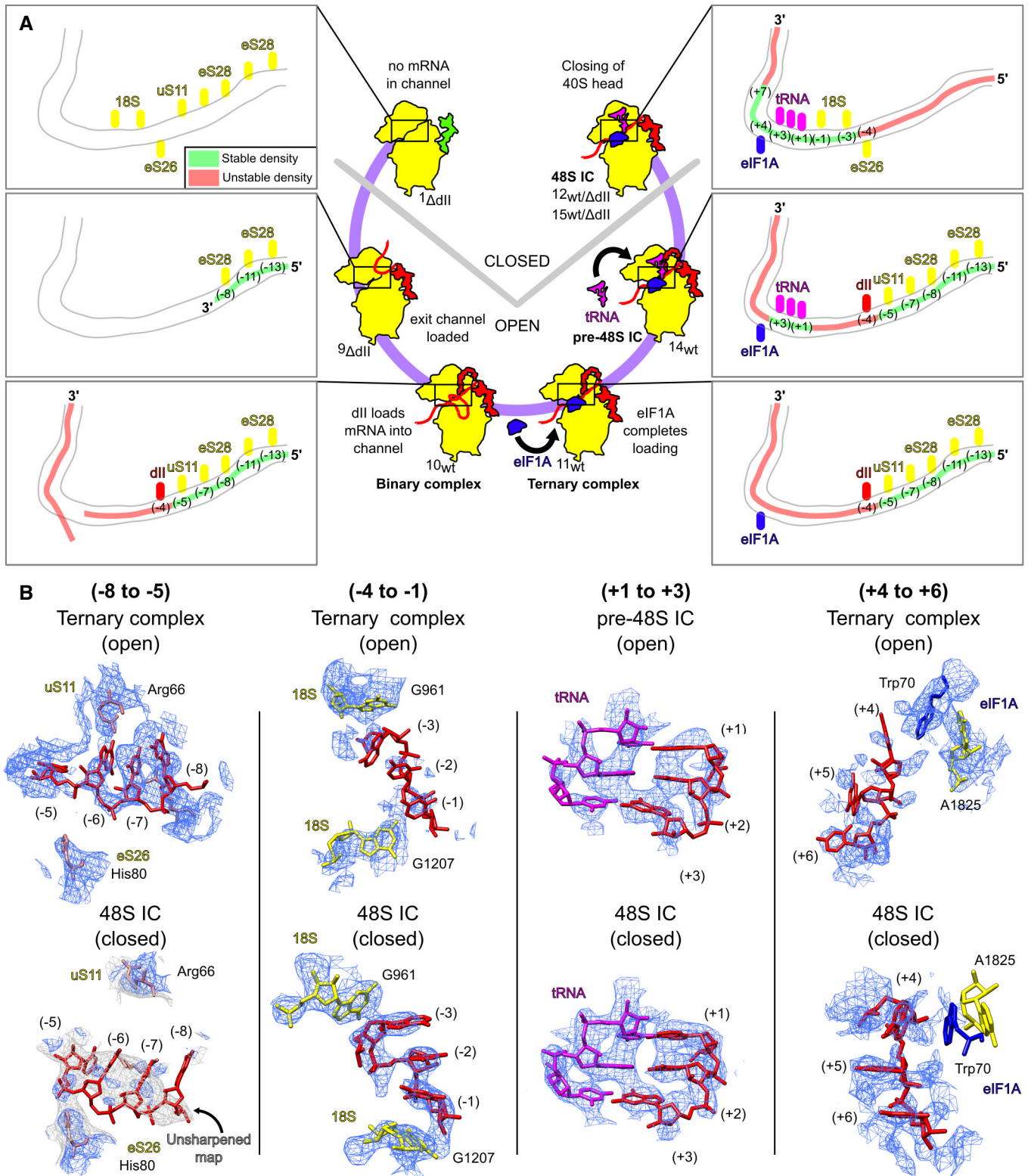


**Figure 6. Ribosomal contacts and stability of mRNA along the mRNA-binding channel at different stages of initiation on the HCV IRES.**

A Occupancy of the mRNA channel for the indicated complexes showing the identity of ribosomal components (yellow), tRNA (magenta), eIF1A (blue), or IRES domain II (red) that interact with mRNA in the mRNA-binding channel. The stability of mRNA in the channel was assessed as either stable (green) or unstable (red) depending on quality of density attributable to each nucleotide.

B Comparison of density maps and models for specific areas of mRNA in the mRNA-binding channel in the indicated open and closed ribosomal complexes.

position, likely due to stabilizing contacts of eS28 residues Arg31 and Arg66 with the (−13)/(−11) and (−8) nucleotides, respectively. In addition, mRNA in the *wt* complex (structure 10<sub>wt</sub>) also forms interactions at the (−7) and (−5) nucleotides with eS28 Arg69 and uS11 Arg66. Although in the unsharpened map, mRNA is visible from the exit through to the P site, the position of each nucleotide was clearly defined only in the (−13) to (−5) nt region where mRNA contacts eS28 and uS11, whereas the downstream region up to position (+2) was more heterogeneous and the quality of the sharpened map declined. In the open 40S/IRES/eIF1A ternary complexes (structure 11<sub>wt</sub>), association with eIF1A resulted in mRNA accommodation in the entire mRNA-binding channel, but it did not influence the mRNA-40S interactions observed in the binary complexes and also did not stabilize the mRNA region from the E to A sites. Establishment of the P-site codon–anticodon interaction in the open eIF5B-containing pre-48S IC (structure 14<sub>wt</sub>) led to stabilization of the P-site codon, resulting in clear density-forming Watson-Crick base pairs with the tRNA anticodon (Fig 5D), but preserved mRNA interactions with eS28 and uS11 and its overall position and conformation observed in the 40S/IRES/eIF1A ternary complex. As in the ternary complex (structure 11<sub>wt</sub>), the presence of eIF1A at high occupancy in pre-48S ICs was not associated with stabilization of the (+4) to (+7) region of mRNA.

The closed-state eIF2- and eIF5B-containing 48S ICs (structure 12<sub>wt/ΔdII</sub>, and 15<sub>wt/ΔdII</sub>) show identical mRNA conformations and stability patterns along the mRNA-binding channel that differ from those observed in the open-state complexes. Due to the head closure, eS28 and uS11 can no longer make contacts with the (−13), (−11), and (−5) nucleotides, and mRNA has moved by ~6 Å toward the body so that eS26 His80 contacts the (−5) nucleotide phosphate backbone. In contrast to the open-state complexes, the new position of mRNA is characterized by the poorly defined region upstream of the (−5) nucleotide, whereas the (−3) to (−1) region is stabilized, forming a stacking triple sandwiched between 18S rRNA G<sub>961</sub> and G<sub>1207</sub>. In all 48S ICs, the P-site codon shows clear density interacting with the tRNA anticodon (Fig 5C and E). In contrast to the pre-48S IC, the presence of eIF1A influences the stability of the (+4) to (+7) nucleotides in 48S ICs. In complexes with high eIF1A occupancy (structures 12<sub>ΔdII</sub>, 15<sub>wt</sub>), the (+4) nucleotide forms a stacking triple with eIF1A Trp70 and 18S rRNA A<sub>1825</sub>, and the (+4) to (+7) region is stable. Such stabilization was not observed in complexes with lower eIF1A occupancy (structures 12<sub>wt</sub>, 15<sub>ΔdII</sub>).

Thus, our data indicate that transition from the open to the closed states is accompanied by changes in mRNA interactions and stability patterns along the mRNA-binding channel. Movement of the 40S subunit head in 48S ICs results in the loss of the interaction between the mRNA region upstream of the (−5) nucleotide with eS28 and uS11 and subsequent destabilization of this region compared with the open-state complexes. On the other hand, the 40S subunit closure leads to stabilization of the (−3) to (−1) mRNA region between 18S rRNA bases. Notably, in closed 48S ICs, but not in open ribosomal complexes, the (+4) to (+7) mRNA region can be stabilized by eIF1A.

### Comparison of eIF5B-containing pre-48S initiation complexes with eIF2-containing scanning 43S complexes

In contrast to initiation on the HCV IRES, eIF5B cannot substitute for eIF2 in recruiting Met-tRNA<sub>i</sub><sup>Met</sup> to the 40S subunit in the

canonical scanning mechanism. Canonical initiation also requires eIF1, which binds to the 40S subunit below the mRNA channel at the P site between h24 and the region connecting h44 to h45 and, in cooperation with eIF1A, stabilizes the open conformation of the 40S subunit (Passmore *et al*, 2007; Ll acer *et al*, 2015), thereby promoting ribosomal attachment to mRNA, scanning and initiation codon selection (e.g., Pestova & Kolupaeva, 2002). Comparison of the eIF5B-containing pre-48S ICs (structure 14<sub>wt</sub>) and canonical scanning, eIF2-containing 43S complexes that also contained eIF1 (Brito Querido *et al*, 2020) revealed that the positions of mRNA and conformations of the anticodon loop of Met-tRNA<sub>i</sub><sup>Met</sup> in the P site in both complexes are very similar (Fig 7A), and the anticodon in the scanning 43S complex is also in a position that enables the establishment of codon–anticodon base pairing (Fig 7B, center panel). However, whereas the conformations of the anticodon in the P site in both complexes are similar, in the eIF5B-containing complex, the T-arm and the acceptor stem are shifted toward the body of the 40S subunit by bending of the anticodon loop region (Fig 7A). Consequently, the contacts between the ASL of Met-tRNA<sub>i</sub><sup>Met</sup> and 18S rRNA nucleotides GA<sub>1639-40</sub> and the N-terminal region of uS9 in the head of the 40S subunit, which are present in all eIF2-containing complexes, including mRNA-free 43S complexes, scanning 43S complexes and 48S ICs (e.g., Hussain *et al*, 2014; Brito Querido *et al*, 2020; Simonetti *et al*, 2020; Fig 7B, center panel), do not exist in the eIF5B-containing pre-48S ICs and only form after ribosomal closure in 48S ICs (Fig 7B, left and right panels). Thus, interaction with eIF2 allows tRNA to maintain the contacts with the head in all 40S subunit conformations, from fully open to fully closed, and the position of the anticodon loop that allows it to inspect mRNA in the scanning 43S complexes is determined by the rotation of the head to a position that is intermediate between fully open and fully closed states. In contrast, in the open pre-48S IC, tRNA is stabilized by contacts between eIF5B domain IV and the acceptor stem, codon–anticodon base pairing, and by stacking of the aromatic rings of ASL C<sub>33</sub> with C<sub>1701</sub> of 18S rRNA (Fig 7B, left panel). Interestingly, in the scanning 43S complex, the C<sub>33</sub> ribose instead forms a lone pair-π interaction with U<sub>1248</sub> of 18S rRNA (Fig 7B, middle panel), whereas in canonical 48S ICs (e.g., Simonetti *et al*, 2020), and in eIF5B-containing 48S ICs (structure 15<sub>wt</sub>), C<sub>33</sub> is involved in both interactions (Fig 7B, right panel). Thus, whereas some aspects of eIF5B-containing pre-48S complexes are analogous to those of eIF2-containing scanning 43S complexes, the overall orientation and the specific interactions of tRNA in them differ.

During eIF2-dependent canonical initiation, the open, scanning-competent conformation of the 40S subunit is determined by the binding of eIF1. We therefore analyzed whether the binding of eIF1 would be compatible with the positions of eIF5B and Met-tRNA<sub>i</sub><sup>Met</sup> in the open pre-48S ICs. The position of eIF1 placed into such complexes suggests that it would clash with tRNA. Thus, the repositioning of tRNA in eIF5B-containing complexes causes the AAC<sub>38-40</sub> nucleotides of Met-tRNA<sub>i</sub><sup>Met</sup> to move toward the 40S subunit body by ~3.0 Å, so that the binding of eIF1 as in the 43S scanning complex would create a clash between A<sub>36</sub> of Met-tRNA<sub>i</sub><sup>Met</sup> and the β1-β2 loop (Fig 7C). Accommodation of eIF1 would require either reorganization of this loop or displacement of the P-site tRNA. Examination of human (Fletcher *et al*, 1999) and yeast (Reibarkh *et al*, 2008) solution NMR structures of eIF1 did not identify any conformations of the β1-β2 loop that would allow a clash with the

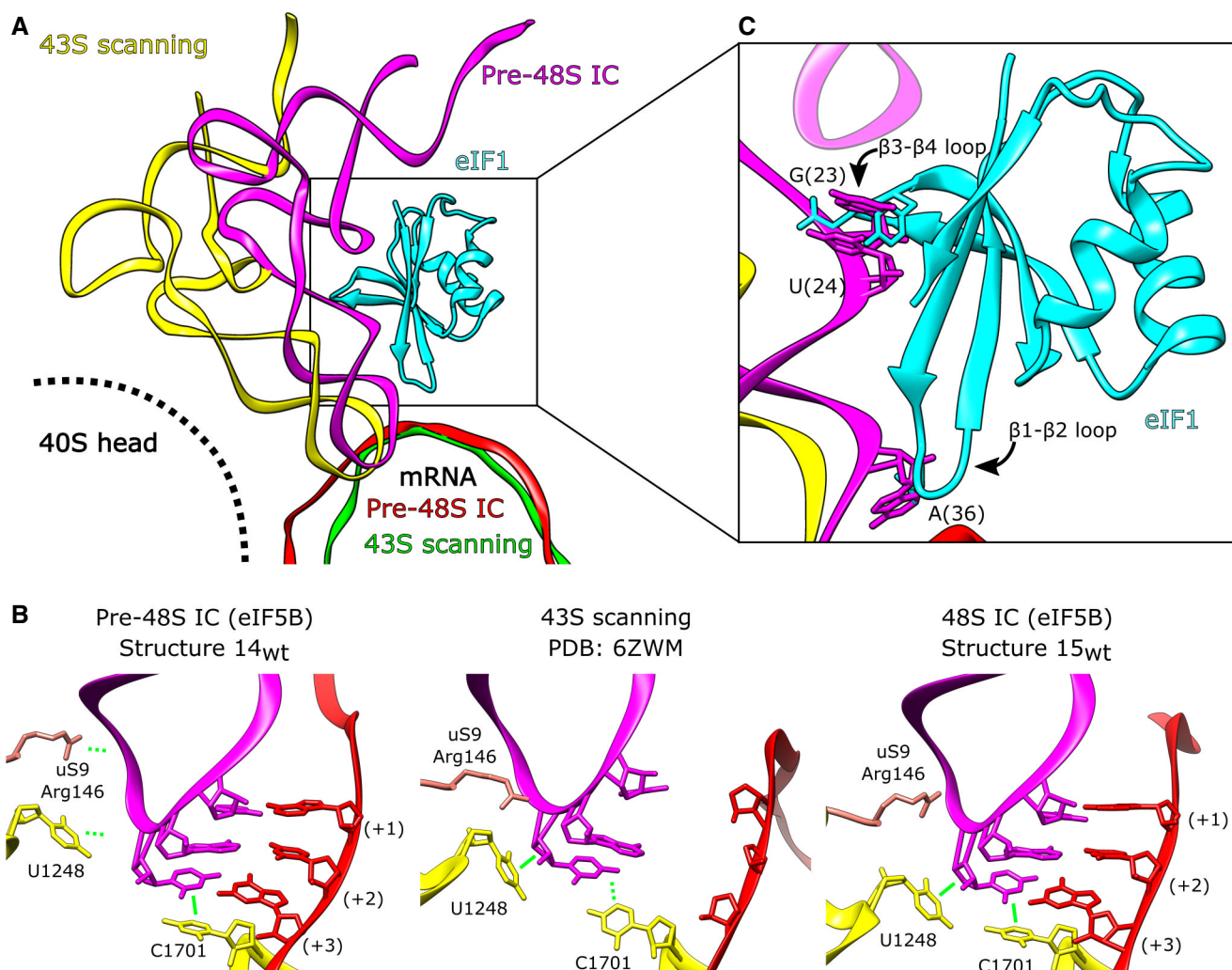


**Figure 7. Position of eIF5B-bound P site Met-tRNA<sup>Met</sup> in open ribosomal complexes is not compatible with eIF1-mediated scanning.**

**A** Position of the P site Met-tRNA<sup>Met</sup> in the scanning 43S complex (PDB: 6ZMW; yellow), and the pre-48S IC (structure 14<sub>wt</sub>; magenta). mRNA from the 43S scanning complex (green) and pre-48S IC (red) is shown. eIF1 associated with the scanning 43S complex is in cyan.

**B** Contacts between tRNA (magenta), the initiation codon (red), and the P site (yellow) for the indicated complexes.

**C** The β1-β2 and β3-β4 loops of eIF1 bound as in the 43S scanning complex (PDB: 6ZMW) would clash with the position of P site Met-tRNA<sup>Met</sup> in eIF5B-containing pre-48S ICs.

anticodon stem of tRNA to be avoided in the eIF5B-containing pre-48S and 48S ICs. Moreover, the eIF1 β3-β4 loop would also clash with tRNA nucleotides GU<sub>23-24</sub>, and a clash between Phe113 and tRNA nucleotide G<sub>25</sub> is also possible (Fig 7C). These observations suggest that even if eIF5B were able to bind Met-tRNA<sup>Met</sup> with high affinity and recruit it to the 40S subunit efficiently, the structure of the resulting complexes would not be compatible with the binding of eIF1 and hence, with the scanning mechanism of initiation. On the other hand, the stabilizing interaction of the acceptor arm of Met-tRNA<sup>Met</sup> with domain IV of eIF5B in the closed 48S complexes following dissociation of eIF1 and eIF2-GDP would lock the complex, preventing leaky scanning from occurring. The incompatibility of Met-tRNA<sup>Met</sup> and eIF1 on eIF5B-containing pre-48S complexes also likely explains why eIF1 disrupts 48S complexes prepared using *wt* but not the ΔII variant of the HCV-like CSFV IRES (Pestova et al, 2008). Domain II has the propensity to insert into the E site

(Quade et al, 2015; Yamamoto et al, 2015; this report), stabilizing the open conformation of the 40S subunit, and if eIF1 binds to this complex, then the insertion of its β1-β2 loop into the mRNA channel creates steric hindrance between mRNA and tRNA in the P site, thereby dislodging the tRNA. We did not identify complexes formed on the ΔII IRES in the open conformation, suggesting that closure is fast in the absence of domain II, so that eIF1 is unable to gain access to such complexes and destabilize them.

## Discussion

Here we present the most comprehensive structural overview of the HCV IRES-mediated initiation pathway to date (Fig 8) that shows the sequential conformational and compositional changes that occur during this process. Initially, the IRES binds to the 40S subunit

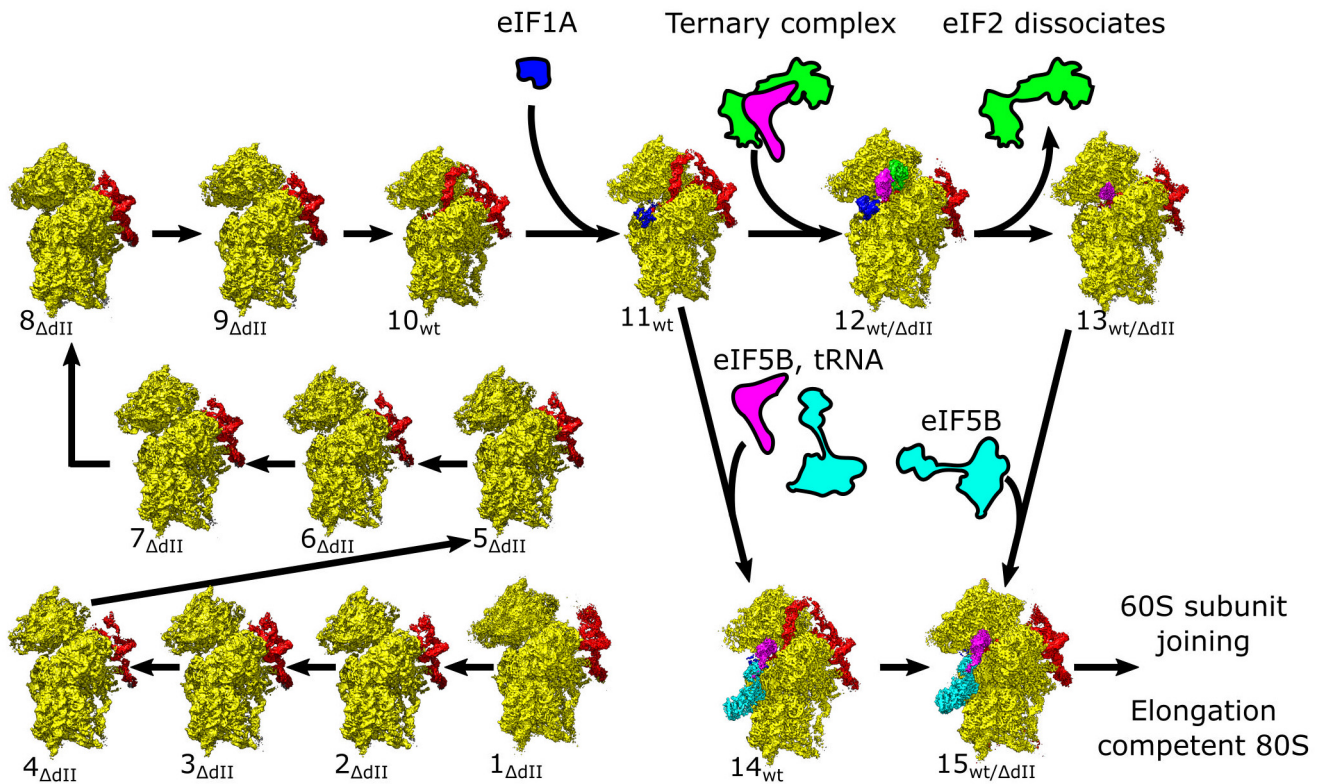


**Figure 8. The HCV IRES-mediated initiation pathway.**

Ribosomal complexes organized in a putative IRES-mediated initiation pathway. Maps are segmented showing the 40S subunit (yellow), IRES (red), eIF1A (blue), Met-tRNA<sup>Met</sup> (magenta), and eIF2 (green) or eIF5B (cyan).

through domains IIIa/IIIc and then pivots onto its platform side where it establishes the complete set of contacts (structures 1<sub>ΔdII</sub>–6<sub>ΔdII</sub>). Formation of the full set of canonical contacts between the IRES domains IIIa/IIIc/IIIId/IIIe/IIIff and the 40S subunit platform riboproteins eS1, eS27, and 18S rRNA ES7 induces the head of the 40S subunit to open (structures 8<sub>ΔdII</sub>–9<sub>ΔdII</sub>). Although head opening can occur in the absence of IRES domain II, such complexes are nevertheless characterized by remarkable heterogeneity in the position of the 40S subunit head. In contrast, 40S/IRES binary complexes assembled on the *wt* IRES yield a uniform structure, in which the 40S subunit is in the open conformation, and domain II is inserted into the E site (structure 10<sub>wt</sub>). Importantly, in the absence of domain II, mRNA density was clearly seen only in the exit portion of the channel up to the (–8) position of mRNA (structure 9<sub>ΔdII</sub>). In the *wt* 40S/IRES binary complex, mRNA nucleotides could be identified at the exit channel through the E site, where it is stabilized by domain II, to AU<sub>342-3</sub> located in the P site (structure 10<sub>wt</sub>), and eIF1A promotes further accommodation of the mRNA in the entire mRNA-binding channel (structure 11<sub>wt</sub>). Thus, complexes (1<sub>ΔdII</sub>–11<sub>wt</sub>) provide structural insights into the functions of multiple IRES domains, including IIIa/IIIc in establishing the initial ribosome contacts, IIIId and IIII<sub>1</sub>/IIIe/IIIff in fixing the IRES to the 40S subunit and inducing ribosomal head opening, and II in imposing the open conformation and promoting fixation of mRNA in and upstream of the P site. Our analysis also revealed the role of eIF1A in completing mRNA accommodation, as prior to eIF1A binding the mRNA is

incompletely loaded into the mRNA channel (structure 10<sub>wt</sub>) and loading is complete only after eIF1A binding (structure 11<sub>wt</sub>).

Once the mRNA is loaded, initiation can proceed either along the canonical initiation pathway, in which eIF2 promotes attachment of Met-tRNA<sup>Met</sup> to form the 48S IC (structure 12<sub>wt/ΔdII</sub>) and then dissociates after GTP hydrolysis (likely structure 13<sub>wt/ΔdII</sub>) followed by binding of eIF5B (structure 15<sub>wt/ΔdII</sub>), or by a shortcut route, in which Met-tRNA<sup>Met</sup> is loaded directly by eIF5B, first forming the open-state pre-48S IC (structure 14<sub>wt</sub>) and then transitioning to the closed 48S IC (structure 15<sub>wt</sub>).

The eIF2-containing 48S IC assembled on the IRES is structurally identical to the canonical 48S IC with respect to the conformation of the 40S subunit and the positions of Met-tRNA<sup>Met</sup>, eIF2, and eIF1A. The position of domain II of the IRES in 40S/IRES<sub>wt</sub> binary complexes is incompatible with the binding of eIF2 and the closed conformation of the 40S subunit, and consequently, in 48S ICs, domain II is oriented away from the subunit interface, toward the solvent side, occupying multiple conformations. In eIF5B-containing pre-48S ICs, the 40S subunit is in the open conformation and domain II is inserted into the E site. Upon 40S subunit closure in eIF5B-containing 48S ICs, domain II becomes displaced from the E site and is again oriented away from the subunit interface like in eIF2-containing 48S ICs. Importantly, compared with eIF2-containing 48S ICs, in eIF5B-containing pre-48S ICs and 48S ICs, Met-tRNA<sup>Met</sup> is rotated by ~14° and moved 15 Å from the head of the 40S subunit to a position that matches its orientation in 80S ribosomes. Thus,

our data show how eIF5B repositions tRNA already on the 48S complex, preparing it for joining with the 60S subunit.

## Materials and Methods

### Plasmids

Vectors for expression of His<sub>6</sub>-tagged eIF1A (Pestova *et al*, 1998a) and *Escherichia coli* methionyl tRNA synthetase (Lomakin *et al*, 2006) have been described. The plasmid HCV-MSTN-Stop (Hashem *et al*, 2013) containing HCV Type 1 nt 40–375 was used for the transcription of mRNA containing the *wt* HCV IRES. A derivative for transcription of HCV IRES lacking domain II (containing HCV nt. 125–375) was made by GenScript Corp. (Piscataway, NJ). The HCV plasmids were linearized by BamHI, and mRNAs were transcribed using T7 RNA polymerase (Thermo Scientific).

### Purification of factors, ribosomal subunits, and aminoacylation of tRNA

Native mammalian 40S subunits, eIF2, eIF3, and eIF5B were purified from rabbit reticulocyte lysate (RRL; Green Hectares), as described (Pisarev *et al*, 2007). Recombinant eIF1A and *E. coli* methionyl tRNA synthetase were expressed and purified from *E. coli* as described (Pisarev *et al*, 2007).

For purification of native rabbit total tRNA, 200 ml RRL were centrifuged at 45,000 rpm (RCF<sub>max</sub> = 244,000 × *g*) for 4.5 h in a Beckman 50.2 Ti rotor at 4°C in order to pellet polysomes. The supernatant was dialyzed overnight against buffer A (20 mM Tris [pH 7.5], 4 mM MgCl<sub>2</sub>, 250 mM KCl, 2 mM DTT) and applied to a DE52 (Whatman) column equilibrated with buffer A. The tRNA was eluted with buffer B (20 mM Tris [pH 7.5], 3 mM MgCl<sub>2</sub>, 700 mM NaCl, 2 mM DTT) and precipitated overnight with 2.5 volumes of ethanol at –80°C. The precipitate was centrifuged at 13,000 rpm (RCF<sub>max</sub> = 20,000 × *g*) for 15 min and resuspended in 5 ml buffer C (100 mM Tris [pH 7.5], 5 mM MgCl<sub>2</sub>), phenol-chloroform (pH 4.7) extracted and precipitated again with 0.3 M NaOAc and 2.5 volumes of ethanol. To isolate tRNA, the pellet was dissolved and subjected to gel filtration on a Superdex 75 column (Pestova & Hellen, 2001). Purified total tRNA was aminoacylated using *E. coli* methionyl tRNA synthetase (to obtain Met-tRNA<sub>i</sub><sup>Met</sup>) as described (Pisarev *et al*, 2007).

### Assembly of ribosomal complexes

To form 48S initiation complexes, 7 pmol HCV IRES mRNA (*wt* or Δdomain II mutant) were incubated with 3.5 pmol 40S subunits, 10 pmol eIF1A, 4.5 pmol eIF3, total native rabbit tRNA containing 3.5 pmol Met-tRNA<sub>i</sub><sup>Met</sup>, and 6 pmol eIF2 or 10 pmol eIF5B in 40 μl buffer D (20 mM Tris [pH 7.5], 100 mM KAc, 2.5 mM MgCl<sub>2</sub>, 2 mM DTT, 0.25 mM spermidine, 1 mM ATP and 0.2 mM GTP) for 10 min at 37°C. The obtained complexes (containing 87.5 nM 40S subunits) were applied directly onto grids without dilution.

### Grid preparation and electron microscopy

Gold foil grids were prepared from Quantifoil gold mesh grids (Passmore & Russo, 2016). Initially, Quantifoil R0.6/1.0300 mesh gold

grids (Quantifoil Micro Tools GmbH) were visually inspected to check for uniformity and intactness of the Quantifoil layer and then placed into an Auto 306 Turbo Vacuum Coater (Edwards Vacuum) at a pressure of 10<sup>3</sup> Pa, and then, gold wire (Ted Pella, Inc) was evaporated for approximately 8 min to create a 500 Å layer. Deposition thickness was determined using the inbuilt film thickness monitor. To remove the underlying Quantifoil carbon foil layer the grids were then treated with plasma using a Gatan Solarus 950 (Gatan, Inc) operated at 25 W for 4 min with an argon/oxygen gas mixture.

To prepare hydrophilic grids, 30 min prior to sample application, grids were treated with plasma using a Gatan Solarus 950 (Gatan, Inc) operated at 25 W for 25 s with a hydrogen/oxygen gas mixture. These grids were then transferred to the environmental chamber of a Vitrobot Mark IV (Thermo Fisher Scientific) maintained at 4°C and 100% humidity. Here, 3 μl of sample was applied and then blotted for 4 s with blot force 3 before plunging into a cooled (77 K) ethane-propane mixture (Tivol *et al*, 2008) and then transferred to liquid nitrogen. Selected grids were screened to confirm sample composition and ice thickness using a Tecnai F20 electron microscope (Thermo Fisher Scientific) equipped with a field emission gun (FEG) operating at 200 kV and a K2 Summit direct electron detector (Gatan, Inc).

After screening grids from each sample, data collection was performed on a Tecnai Polara F30 (Thermo Fisher Scientific) equipped with an FEG operating at 300 kV and a K3 direct electron detector (Gatan, Inc). Movies were collected at a nominal magnification of 52,000× and defocus range of –0.5 to –2.5 μm in counting mode with a pixel size of 0.95 Å using the automated collection software Leginon (Potter *et al*, 1999; Carragher *et al*, 2000; Suloway *et al*, 2005). Each movie consisted of 40 frames recorded over 4 s with a total dose of 70.9 e<sup>–</sup>/Å<sup>2</sup>. Due to sample conditions, the 40S ribosomal subunits were observed in a preferred orientation, and so, portions of the data were collected with a 30° stage tilt (Appendix Table S2). For the *wt* IRES eIF2-containing sample 14,815 micrographs (14,815 at 30° stage tilt) were collected over two sessions, for the *wt* IRES eIF5B-containing sample 27,263 micrographs (20,509 at 30° stage tilt) were collected over four sessions, for the ΔII IRES eIF2-containing sample 22,735 micrographs (17,695 at 30° stage tilt) were collected over three sessions, and for the ΔII IRES eIF5B-containing sample 13,809 micrographs (13,809 at 30° stage tilt) were collected over two sessions (Appendix Table S2). Optical groups of micrographs with similar beam tilt values were identified using k-means clustering on the image shift values recorded by the microscope during data collection.

### Image processing

Gain references for each session were produced by visually screening ~1,000 micrographs to remove images that contained gold foil and then summing them using cisTEM *sum\_all\_tifs* (Grant *et al*, 2018). Movies were then aligned using MotionCor2 (Zheng *et al*, 2017) with dose weighting of 1.77 e<sup>–</sup>/Å<sup>2</sup>/frame and local patch correction with 8 × 5 patches. Initial CTF parameters were estimated using CTFIND4 (Rohou & Grigorieff, 2015). Particle locations were identified using Topaz version 0.2.3 (Bepler *et al*, 2019) by initially downscaling all micrographs by 8× and then using the Topaz general model to identify particles. Particles with a

confidence score below 0 were removed and the remaining positions rescaled for subsequent processing in Relion 3.1 (Scheres, 2012, 2016; Zivanov et al, 2018, 2019).

Initially, we identified 2,183,185 particles for the *wt* IRES eIF2-containing sample (147 particles per micrograph), 1,133,335 particles for the *wt* IRES eIF5B-containing sample (42 particles per micrograph), 2,213,826 particles for the  $\Delta$ dII IRES eIF2-containing sample (97 particles per micrograph), and 1,459,506 particles for the  $\Delta$ dII IRES eIF5B-containing sample (106 particles per micrograph). Particle locations were extracted from micrographs into downsampled boxes of  $100 \times 100$  pixels (at  $3.8 \text{ \AA}/\text{pixel}$ ) to speed up initial classification. This corresponds to  $400 \times 400$ -pixel boxes (at  $0.95 \text{ \AA}/\text{pixel}$ ) without downsampling. Twenty-five iterations of 2D classification were performed to identify incorrectly-picked particles, contamination, and other particles that were unable to be correctly aligned (e.g., due to poor signal-to-noise). Particles that were selected for removal were subjected to additional 2D classification to confirm that they did not contain clear 40S ribosome particles.

After the initial screening of the 2D classification data, the remaining particles for each sample were 1,201,923 particles for the *wt* IRES eIF2-containing sample (81 particles per micrograph), 736,700 particles for the *wt* IRES eIF5B-containing sample (36 particles per micrograph), 1,484,658 particles for the  $\Delta$ dII IRES eIF2-containing sample (84 particles per micrograph), and 1,119,610 particles for the  $\Delta$ dII IRES eIF5B-containing sample (81 particles per micrograph). For each sample, all particles were refined into a single model, which was used to estimate the defocus values on a per-particle basis, followed by an additional refinement step, and then 3D classification without alignment into 10 classes for 25 iterations. This initial 3D classification was used to identify the major conformational states present in each sample, and further removal of poor-quality particles. For the *wt* IRES eIF2-containing sample, we identified 580,938 particles in the closed state, 176,793 particles in the open state, and removed 444,192 particles. For the *wt* IRES eIF5B-containing sample, we identified 378,325 open state, 360,338 closed state, and removed 58,037 particles. For the  $\Delta$ dII IRES eIF5B-containing sample, we identified 883,893 particles in the closed state and removed 62,455 particles. For the  $\Delta$ dII IRES eIF2-containing sample, we identified 615,125 particles in the closed state, 198,920 particles in the intermediate-open state, and removed 670,433 particles. All particles that were selected for removal were subjected to additional 2D classification and 3D refinement steps to confirm that they did not contain 40S ribosome complexes.

### General processing pathway

All particles were re-extracted at full-size ( $400 \times 400$  pixel box,  $0.95 \text{ \AA}/\text{pixel}$ ) and underwent iterations of 3D refinement, followed by anisotropic magnification correction, defocus refinement, and beam tilt estimation. Multiple rounds of 3D classification (25 iterations, without alignment) were used to progressively remove poor-quality particles. After each round of CTF refinement, each particle stack underwent 3D refinement and was checked for an increase in resolution and visual improvement of map density. Once CTF refinement no longer improved map quality, particle polishing using all frames was performed and then iterations of CTF refinement as outlined above were completed. Focused classification on consensus

maps was performed to isolate desired conformational or compositional states. Full details of the processing pathway for each complex are included in the expanded information available online.

### Model building and refinement

For all data, where applicable, we were able to unambiguously fit the head and body of the 40S (PDB: 6D9J; Pisareva et al, 2018), HCV IRES (PDB: 5FLX; Yamamoto et al, 2015), eIF1A (PDB: 4KZZ; Lomakin & Steitz, 2013), tRNA (PDB: 5K0Y; Simonetti et al, 2016) eIF2 $\alpha$  subunit (PDB: 6O85; Kenner et al, 2019), and eIF5B (PDB: 4UJD; Yamamoto et al, 2014). Initial model fitting was performed using UCSF Chimera v1.14 (Pettersen et al, 2004) with additional modeling in Coot (Emsley & Cowtan, 2004). For regions of eIF5B that did not have available models (e.g., Switch 1), model building was performed independently and then cross-checked for consistency. All models underwent one round of Phenix geometry minimization and multiple rounds of PHENIX real-space refinement (Adams et al, 2010; Afonine et al, 2018).

### Data availability

Primary models and maps (Appendix Table S3) reported in this study were deposited in the Protein Data Bank (PDB) and Electron Microscopy Data Bank (EMDB) under the following accession codes: structure 1 $_{\Delta$ dII (PDB: 7SYG, <https://www.rcsb.org/structure/7SYG>; EMD-25527, <https://www.ebi.ac.uk/emdb/EMD-25527>), structure 2 $_{\Delta$ dII (PDB: 7SYH, <https://www.rcsb.org/structure/7SYH>; EMD-25528, <https://www.ebi.ac.uk/emdb/EMD-25528>), structure 3 $_{\Delta$ dII (PDB: 7SYI, <https://www.rcsb.org/structure/7SYI>; EMD-25529, <https://www.ebi.ac.uk/emdb/EMD-25529>), structure 4 $_{\Delta$ dII (PDB: 7SYJ, <https://www.rcsb.org/structure/7SYJ>; EMD-25530, <https://www.ebi.ac.uk/emdb/EMD-25530>), structure 5 $_{\Delta$ dII (PDB: 7SYK, <https://www.rcsb.org/structure/7SYK>; EMD-25531, <https://www.ebi.ac.uk/emdb/EMD-25531>), structure 6 $_{\Delta$ dII (PDB: 7SYL, <https://www.rcsb.org/structure/7SYL>; EMD-25532, <https://www.ebi.ac.uk/emdb/EMD-25532>), structure 7 $_{\Delta$ dII (PDB: 7SYM, <https://www.rcsb.org/structure/7SYM>; EMD-25533, <https://www.ebi.ac.uk/emdb/EMD-25533>), structure 8 $_{\Delta$ dII (PDB: 7SYN, <https://www.rcsb.org/structure/7SYN>; EMD-25534, <https://www.ebi.ac.uk/emdb/EMD-25534>), structure 9 $_{\Delta$ dII (PDB: 7SYO, <https://www.rcsb.org/structure/7SYO>; EMD-25535, <https://www.ebi.ac.uk/emdb/EMD-25535>), structure 10 $_{wt}$  (PDB: 7SYP, <https://www.rcsb.org/structure/7SYP>; EMD-25536, <https://www.ebi.ac.uk/emdb/EMD-25536>), structure 11 $_{wt}$  (PDB: 7SYQ, <https://www.rcsb.org/structure/7SYQ>; EMD-25537, <https://www.ebi.ac.uk/emdb/EMD-25537>), structure 12 $_{wt}$  (PDB: 7SYR, <https://www.rcsb.org/structure/7SYR>; EMD-25538, <https://www.ebi.ac.uk/emdb/EMD-25538>), structure 12 $_{\Delta$ dII (PDB: 7SYS, <https://www.rcsb.org/structure/7SYS>; EMD-25539, <https://www.ebi.ac.uk/emdb/EMD-25539>), structure 13 $_{wt}$  (PDB: 7SYT, <https://www.rcsb.org/structure/7SYT>; EMD-25540, <https://www.ebi.ac.uk/emdb/EMD-25540>), structure 13 $_{\Delta$ dII (PDB: 7SYU, <https://www.rcsb.org/structure/7SYU>; EMD-25541, <https://www.ebi.ac.uk/emdb/EMD-25541>), structure 14 $_{wt}$  (PDB: 7SYV, <https://www.rcsb.org/structure/7SYV>; EMD-25542, <https://www.ebi.ac.uk/emdb/EMD-25542>), structure 15 $_{wt}$  (PDB: 7SYW, <https://www.rcsb.org/structure/7SYW>).



structure/7SYW; EMD-25543, <https://www.ebi.ac.uk/emdb/EMD-25543>), and structure 15<sub>ΔdII</sub> (PDB: 7SYX, <https://www.rcsb.org/structure/7SYX>; EMD-25544, <https://www.ebi.ac.uk/emdb/EMD-25544>). Additional maps (Appendix Table S5) showing the movement of HCV IRES domain II were deposited in the EMDB under the following accession codes: structure 16<sub>wt</sub> (EMD-25545, <https://www.ebi.ac.uk/emdb/EMD-25545>), structure 17<sub>wt</sub> (EMD-25546, <https://www.ebi.ac.uk/emdb/EMD-25546>), structure 18<sub>wt</sub> (EMD-25547, <https://www.ebi.ac.uk/emdb/EMD-25547>), structure 19<sub>wt</sub> (EMD-25548, <https://www.ebi.ac.uk/emdb/EMD-25548>), structure 20<sub>wt</sub> (EMD-25549, <https://www.ebi.ac.uk/emdb/EMD-25549>), structure 21<sub>wt</sub> (EMD-25550, <https://www.ebi.ac.uk/emdb/EMD-25550>), structure 22<sub>wt</sub> (EMD-25551, <https://www.ebi.ac.uk/emdb/EMD-25551>), structure 23<sub>wt</sub> (EMD-25552, <https://www.ebi.ac.uk/emdb/EMD-25552>), structure 24<sub>wt</sub> (EMD-25553, <https://www.ebi.ac.uk/emdb/EMD-25553>), structure 25<sub>wt</sub> (EMD-25554, <https://www.ebi.ac.uk/emdb/EMD-25554>), structure 26<sub>wt</sub> (EMD-25555, <https://www.ebi.ac.uk/emdb/EMD-25555>), structure 27<sub>wt</sub> (EMD-25556, <https://www.ebi.ac.uk/emdb/EMD-25556>), and structure 28<sub>wt</sub> (EMD-25557, <https://www.ebi.ac.uk/emdb/EMD-25557>). Maps obtained during data processing (Appendix Table S7) from particle stacks that were compositionally and conformationally identical and were later combined were deposited in the EMDB under the following accession codes: structure 29<sub>wt</sub> (EMD-25588, <https://www.ebi.ac.uk/emdb/EMD-25588>), structure 30<sub>wt</sub> (EMD-25589, <https://www.ebi.ac.uk/emdb/EMD-25589>), structure 31<sub>ΔdII</sub> (EMD-25590, <https://www.ebi.ac.uk/emdb/EMD-25590>), and structure 32<sub>ΔdII</sub> (EMD-25591, <https://www.ebi.ac.uk/emdb/EMD-25591>). Consensus maps (Appendix Table S7) that were used for focused classification were deposited in the EMDB under the following accession codes: structure 33<sub>ΔdII</sub> (EMD-25592, <https://www.ebi.ac.uk/emdb/EMD-25592>), structure 34<sub>ΔdII</sub> (EMD-25593, <https://www.ebi.ac.uk/emdb/EMD-25593>), structure 35<sub>wt</sub> (EMD-25594, <https://www.ebi.ac.uk/emdb/EMD-25594>), structure 36<sub>wt</sub> (EMD-25595, <https://www.ebi.ac.uk/emdb/EMD-25595>), structure 37<sub>ΔdII</sub> (EMD-25596, <https://www.ebi.ac.uk/emdb/EMD-25596>), structure 38<sub>wt</sub> (EMD-25597, <https://www.ebi.ac.uk/emdb/EMD-25597>), structure 39<sub>wt</sub> (EMD-25598, <https://www.ebi.ac.uk/emdb/EMD-25598>), and structure 40<sub>ΔdII</sub> (EMD-25599, <https://www.ebi.ac.uk/emdb/EMD-25599>). Other high-resolution maps obtained during classification were deposited in the EMDB under the following accession codes: structure 41<sub>wt</sub> (EMD-25600, <https://www.ebi.ac.uk/emdb/EMD-25600>), structure 42<sub>wt</sub> (EMD-25601, <https://www.ebi.ac.uk/emdb/EMD-25601>), structure 43<sub>wt</sub> (EMD-25602, <https://www.ebi.ac.uk/emdb/EMD-25602>), structure 44<sub>wt</sub> (EMD-25603, <https://www.ebi.ac.uk/emdb/EMD-25603>), structure 45<sub>wt</sub> (EMD-25604, <https://www.ebi.ac.uk/emdb/EMD-25604>), and structure 46<sub>ΔdII</sub> (EMD-25620, <https://www.ebi.ac.uk/emdb/EMD-25620>). For each entry, the half maps, unsharpened map, mask used for postprocessing, and the Fourier correlation curve has been deposited as additional files. Primary map entries also have local resolution maps as additional files and consensus map entries have the focused classification masks included. Requests for materials and additional information can be directed to Dr. Tatyana Pestova (tatyana.pestova@downstate.edu) or Dr. Joachim Frank (jf2192@cumc.columbia.edu).

**Expanded View** for this article is available online.

## Acknowledgements

This work was supported by grants from the National Institutes of Health (National Institute of General Medical Sciences), R01 GM55440 (to JF), R35 GM139453 (to JF), R35 GM122602 (to TVP), and R01 GM097014 (to CUTH), and from the National Institutes of Health (National Institute of Allergy and Infectious Diseases), R01 AI123406 (to CUTH).

## Author contributions

**Zuben P Brown:** Conceptualization; data curation; software; formal analysis; investigation; writing – original draft; writing – review and editing.

**Irina S Abaeva:** Investigation; methodology; writing – review and editing.

**Swastik De:** Investigation; writing – review and editing. **Christopher UT Hellen:** Conceptualization; resources; data curation; formal analysis; supervision; funding acquisition; validation; investigation; methodology; writing – original draft; project administration; writing – review and editing.

**Tatyana V Pestova:** Conceptualization; resources; data curation; formal analysis; supervision; funding acquisition; validation; investigation; methodology; writing – original draft; project administration; writing – review and editing. **Joachim Frank:** Conceptualization; resources; data curation; formal analysis; supervision; funding acquisition; validation; investigation; methodology; writing – original draft; project administration; writing – review and editing.

## Disclosure and competing interests statement

The authors declare that they have no conflict of interest.

## References

- Acker MG, Shin BS, Dever TE, Lorsch JR (2006) Interaction between eukaryotic initiation factors 1A and 5B is required for efficient ribosomal subunit joining. *J Biol Chem* 281: 8469–8475
- Adams PD, Afonine PV, Bunkóczi G, Chen VB, Davis IW, Echols N, Headd JJ, Hung LW, Kapral GJ, Grosse-Kunstleve RW *et al* (2010) PHENIX: a comprehensive python-based system for macromolecular structure solution. *Acta Crystallogr D Biol Crystallogr* 66: 213–221
- Afonine PV, Poon BK, Read RJ, Sobolev OV, Terwilliger TC, Urzhumtsev A, Adams PD (2018) Real-space refinement in PHENIX for cryo-EM and crystallography. *Acta Crystallogr D Biol Crystallogr* 74: 531–544
- Angulo J, Ulryck N, Deforges J, Chamond N, Lopez-Lastra M, Masquida B, Sargueil B (2016) LOOP IIIId of the HCV IRES is essential for the structural rearrangement of the 40S-HCV IRES complex. *Nucleic Acids Res* 44: 1309–1325
- Arhah Y, Bulakhov AG, Pestova TV, Hellen CUT (2020) Dissemination of internal ribosomal entry sites (IRES) between viruses by horizontal gene transfer. *Viruses* 12: 612
- Arhah Y, Miścicka A, Pestova TV, Hellen CUT (2022) Horizontal gene transfer as a mechanism for the promiscuous acquisition of distinct classes of IRES by avian caliciviruses. *Nucleic Acids Res* 22: 1052–1068
- Battiste JL, Pestova TV, Hellen CU, Wagner G (2000) The eIF1A solution structure reveals a large RNA-binding surface important for scanning function. *Mol Cell* 5: 109–119
- Bepler T, Morin A, Rapp M, Brasch J, Shapiro L, Noble AJ, Berger B (2019) Positive-unlabeled convolutional neural networks for particle picking in cryo-electron micrographs. *Nat Methods* 16: 1153–1160
- Boehringer D, Thermann R, Ostareck-Lederer A, Lewis JD, Stark H (2005) Structure of the hepatitis C virus IRES bound to the human 80S ribosome: remodeling of the HCV IRES. *Structure* 13: 1695–1706

- Brito Querido J, Sokabe M, Kraatz S, Gordiyenko Y, Skehel JM, Fraser CS, Ramakrishnan V (2020) Structure of a human 48S translational initiation complex. *Science* 369: 1220–1227
- Carragher B, Kisseberth N, Kriegman D, Milligan RA, Potter CS, Pulokas J, Reilein A (2000) Legimon: an automated system for acquisition of images from vitreous ice specimens. *J Struct Biol* 132: 33–45
- de Breyne S, Yu Y, Pestova TV, Hellen CU (2008) Factor requirements for translation initiation on the simian picornavirus internal ribosomal entry site. *RNA* 14: 367–380
- des Georges A, Dhote V, Kuhn L, Hellen CU, Pestova TV, Frank J, Hashem Y (2015) Structure of mammalian eIF3 in the context of the 43S preinitiation complex. *Nature* 525: 491–495
- d'Imprima E, Floris D, Joppe M, Sánchez R, Grininger M, Kühlbrandt W (2019) Protein denaturation at the air-water interface and how to prevent it. *eLife* 8: e42747
- Emsley P, Cowtan K (2004) Coot: model-building tools for molecular graphics. *Acta Crystallogr D Biol Crystallogr* 60: 2126–2132
- Filbin ME, Kieft JS (2011) HCV IRES domain IIb affects the configuration of coding RNA in the 40S subunit's decoding groove. *RNA* 17: 1258–1273
- Fletcher CM, Pestova TV, Hellen CU, Wagner G (1999) Structure and interactions of the translation initiation factor eIF1. *EMBO J* 18: 2631–2637
- Glaeser RM (2021) Preparing better samples for cryo-electron microscopy: biochemical challenges do not end with isolation and purification. *Annu Rev Biochem* 90: 451–474
- Grant T, Rohou A, Grigorieff N (2018) cisTEM, user-friendly software for single-particle image processing. *eLife* 7: e35383
- Hashem Y, des Georges A, Dhote V, Langlois R, Liao HY, Grassucci RA, Pestova TV, Hellen CU, Frank J (2013) Hepatitis-C-virus-like internal ribosome entry sites displace eIF3 to gain access to the 40S subunit. *Nature* 503: 539–543
- Honda M, Ping LH, Rijnbrand RC, Amphlett E, Clarke B, Rowlands D, Lemon SM (1996) Structural requirements for initiation of translation by internal ribosome entry within genome-length hepatitis C virus RNA. *Virology* 222: 31–42
- Huang BY, Fernández IS (2020) Long-range interdomain communications in eIF5B regulate GTP hydrolysis and translation initiation. *Proc Natl Acad Sci USA* 117: 1429–1437
- Hussain T, Llácer JL, Fernández IS, Munoz A, Martin-Marcos P, Savva CG, Lorsch JR, Hinnebusch AG, Ramakrishnan V (2014) Structural changes enable start codon recognition by the eukaryotic translation initiation complex. *Cell* 159: 597–607
- Hussain T, Llácer JL, Wimberly BT, Kieft JS, Ramakrishnan V (2016) Large-scale movements of IF3 and tRNA during bacterial translation initiation. *Cell* 167: 133–144
- Jaafar ZA, Oguro A, Nakamura Y, Kieft JS (2016) Translation initiation by the hepatitis C virus IRES requires eIF1A and ribosomal complex remodeling. *eLife* 5: e21198
- Jackson RJ, Hellen CU, Pestova TV (2010) The mechanism of eukaryotic translation initiation and principles of its regulation. *Nat Rev Mol Cell Biol* 11: 113–127
- Ji H, Fraser CS, Yu Y, Leary J, Doudna JA (2004) Coordinated assembly of human translation initiation complexes by the hepatitis C virus internal ribosome entry site RNA. *Proc Natl Acad Sci USA* 101: 16990–16995
- Jumper J, Evans R, Pritzel A, Green T, Figurnov M, Ronneberger O, Tunyasuvunakool K, Bates R, Žídek A, Potapenko A et al (2021) Highly accurate protein structure prediction with AlphaFold. *Nature* 596: 583–589
- Kaledhonkar S, Fu Z, Caban K, Li W, Chen B, Sun M, Gonzalez RL, Frank J (2019) Late steps in bacterial translation initiation visualized using time-resolved cryo-EM. *Nature* 570: 400–404
- Kenner LR, Anand AA, Nguyen HC, Myasnikov AG, Klose CJ, McGeever LA, Tsai JC, Miller-Vedam LE, Walter P, Frost A (2019) eIF2B-catalyzed nucleotide exchange and phosphoregulation by the integrated stress response. *Science* 364: 491–495
- Kieft JS, Zhou K, Jubin R, Doudna JA (2001) Mechanism of ribosome recruitment by hepatitis C IRES RNA. *RNA* 7: 194–206
- Kolupaeva VG, Pestova TV, Hellen CU (2000) An enzymatic footprinting analysis of the interaction of 40S ribosomal subunits with the internal ribosomal entry site of hepatitis C virus. *J Virol* 74: 6242–6250
- Kuhle B, Ficner R (2014) eIF5B employs a novel domain release mechanism to catalyze ribosomal subunit joining. *EMBO J* 33: 1177–1191
- Llácer JL, Hussain T, Marler L, Aitken CE, Thakur A, Lorsch JR, Hinnebusch AG, Ramakrishnan V (2015) Conformational differences between open and closed states of the eukaryotic translation initiation complex. *Mol Cell* 59: 399–412
- Locker N, Easton LE, Lukavsky PJ (2007) HCV and CSFV IRES domain II mediate eIF2 release during 80S ribosome assembly. *EMBO J* 26: 795–805
- Lomakin IB, Steitz TA (2013) The initiation of mammalian protein synthesis and mRNA scanning mechanism. *Nature* 500: 307–311
- Lomakin IB, Shirokikh NE, Yusupov MM, Hellen CU, Pestova TV (2006) The fidelity of translation initiation: reciprocal activities of eIF1, IF3 and YciH. *EMBO J* 25: 196–210
- Ma P, Ma XX, Chang QY, Li LJ, Wang YN, Feng YP, Ma ZR, Zhou JH (2018) The effects of nucleotide usage in key nucleotide positions +4 and –3 flanking start codon on translation levels mediated by IRES of hepatitis C virus. *Acta Virol* 62: 441–446
- Maag D, Fekete CA, Gryczynski Z, Lorsch JR (2005) A conformational change in the eukaryotic translation preinitiation complex and release of eIF1 signal recognition of the start codon. *Mol Cell* 17: 265–275
- Malygin AA, Kossinova OA, Shatsky IN, Karpova GG (2013a) HCV IRES interacts with the 18S rRNA to activate the 40S ribosome for subsequent steps of translation initiation. *Nucleic Acids Res* 41: 8706–8714
- Malygin AA, Shatsky IN, Karpova GG (2013b) Proteins of the human 40S ribosomal subunit involved in hepatitis C IRES binding as revealed from fluorescent labeling. *Biochemistry (Mosc)* 78: 53–59
- Marintchev A, Kolupaeva VG, Pestova TV, Wagner G (2003) Mapping the binding interface between human eukaryotic initiation factors 1A and 5B: a new interaction between old partners. *Proc Natl Acad Sci USA* 100: 1535–1440
- Matsuda D, Mauro VP (2014) Base pairing between hepatitis C virus RNA and 18S rRNA is required for IRES-dependent translation initiation in vivo. *Proc Natl Acad Sci USA* 111: 15385–15389
- Nag N, Lin KY, Edmonds KA, Yu J, Nadkarni D, Marintcheva B, Marintchev A (2016) eIF1A/eIF5B interaction network and its functions in translation initiation complex assembly and remodeling. *Nucleic Acids Res* 44: 7441–7456
- Neupane R, Pisareva VP, Rodriguez CF, Pisarev AV, Fernández IS (2020) A complex IRES at the 5'-UTR of a viral mRNA assembles a functional 48S complex via an uAUG intermediate. *eLife* 9: e54575
- Odreman-Macchioli F, Baralle FE, Buratti E (2001) Mutational analysis of the different bulge regions of hepatitis C virus domain II and their influence on internal ribosome entry site translational ability. *J Biol Chem* 276: 41648–41655

- Ogle JM, Murphy FV IV, Tarry MJ, Ramakrishnan V (2002) Selection of tRNA by the ribosome requires a transition from an open to a closed form. *Cell* 111: 721–732
- Passmore LA, Russo CJ (2016) Specimen preparation for high-resolution Cryo-EM. *Methods Enzymol* 579: 51–86
- Passmore LA, Schmeing TM, Maag D, Applefield DJ, Acker MG, Algire MA, Lorsch JR, Ramakrishnan V (2007) The eukaryotic translation initiation factors eIF1 and eIF1A induce an open conformation of the 40S ribosome. *Mol Cell* 26: 41–50
- Pestova TV, Hellen CU (2001) Preparation and activity of synthetic unmodified mammalian tRNA<sup>i(met)</sup> in initiation of translation in vitro. *RNA* 7: 1496–1505
- Pestova TV, Kolupaeva VG (2002) The roles of individual eukaryotic translation initiation factors in ribosomal scanning and initiation codon selection. *Genes Dev* 16: 2906–2922
- Pestova TV, Borukhov SI, Hellen CU (1998a) Eukaryotic ribosomes require initiation factors 1 and 1A to locate initiation codons. *Nature* 394: 854–859
- Pestova TV, Shatsky IN, Fletcher SP, Jackson RJ, Hellen CU (1998b) A prokaryotic-like mode of cytoplasmic eukaryotic ribosome binding to the initiation codon during internal translation initiation of hepatitis C and classical swine fever virus RNAs. *Genes Dev* 12: 67–83
- Pestova TV, Lomakin IB, Lee JH, Choi SK, Dever TE, Hellen CU (2000) The joining of ribosomal subunits in eukaryotes requires eIF5B. *Nature* 403: 332–335
- Pestova TV, de Breynne S, Pisarev AV, Abaeva IS, Hellen CU (2008) eIF2-dependent and eIF2-independent modes of initiation on the CSFV IRES: a common role of domain II. *EMBO J* 27: 1060–1072
- Pettersen EF, Goddard TD, Huang CC, Couch GS, Greenblatt DM, Meng EC, Ferrin TE (2004) UCSF Chimera—a visualization system for exploratory research and analysis. *J Comput Chem* 25: 1605–1612
- Pisarev AV, Kolupaeva VG, Pisareva VP, Merrick WC, Hellen CU, Pestova TV (2006) Specific functional interactions of nucleotides at key –3 and +4 positions flanking the initiation codon with components of the mammalian 48S translation initiation complex. *Genes Dev* 20: 624–636
- Pisarev AV, Unbehaun A, Hellen CU, Pestova TV (2007) Assembly and analysis of eukaryotic translation initiation complexes. *Methods Enzymol* 430: 147–177
- Pisareva VP, Pisarev AV, Fernández IS (2018) Dual tRNA mimicry in the cricket paralysis virus IRES uncovers an unexpected similarity with the hepatitis C virus IRES. *eLife* 7: e34062
- Potter CS, Chu H, Frey B, Green C, Kisseberth N, Madden TJ, Miller KL, Nahrstedt K, Pulokas J, Reilein A et al (1999) Legimon: a system for fully automated acquisition of 1000 electron micrographs a day. *Ultramicroscopy* 77: 153–161
- Prince JB, Taylor BH, Rhurlow DL, Ofengand J, Zimmermann RA (1982) Covalent crosslinking of tRNA<sup>Val</sup> to 16S RNA at the ribosomal P site: identification of crosslinked residues. *Proc Natl Acad Sci USA* 79: 5450–5454
- Quade N, Boehringer D, Leibundgut M, van den Heuvel J, Ban N (2015) Cryo-EM structure of hepatitis C virus IRES bound to the human ribosome at 3.9-Å resolution. *Nat Commun* 6: 7646
- Reibarkh, M, Yamamoto, Y, Singh, C.R, del Rio, F, Fahmy, A, Lee, B, Luna, RE, li, M, Wagner, G, and Asano, K (2008) Eukaryotic initiation factor (eIF) 1 carries two distinct eIF5-binding faces important for multifactor assembly and AUG selection. *J Biol Chem* 283: 1094–1103
- Reynolds JE, Kaminski A, Carroll AR, Clarke BE, Rowlands DJ, Jackson RJ (1996) Internal initiation of translation of hepatitis C virus RNA: The ribosome entry site is at the authentic initiation codon. *RNA* 2: 867–878
- Rohou A, Grigorieff N (2015) CTFIND4: fast and accurate defocus estimation from electron micrographs. *J Struct Biol* 192: 216–221
- Scheres SH (2012) RELION: implementation of a Bayesian approach to cryo-EM structure determination. *J Struct Biol* 180: 519–530
- Scheres SH (2016) Processing of structurally heterogeneous cryo-EM data in RELION. *Methods Enzymol* 579: 125–157
- Simonetti A, Brito Querido J, Myasnikov AG, Mancera-Martinez E, Renaud A, Kuhn L, Hashem Y (2016) eIF3 peripheral subunits rearrangement after mRNA binding and start-codon recognition. *Mol Cell* 63: 206–217
- Simonetti A, Guca E, Bochler A, Kuhn L, Hashem Y (2020) Structural insights into the mammalian late-stage initiation complexes. *Cell Rep* 31: 107497
- Sizova DV, Kolupaeva VG, Pestova TV, Shatsky IN, Hellen CU (1998) Specific interaction of eukaryotic translation initiation factor 3 with the 5' nontranslated regions of hepatitis C virus and classical swine fever virus RNAs. *J Virol* 72: 4775–4782
- Spahn CM, Kieft JS, Grassucci RA, Penczek PA, Zhou K, Doudna JA, Frank J (2001) Hepatitis C virus IRES RNA-induced changes in the conformation of the 40S ribosomal subunit. *Science* 291: 1959–1962
- Suloway C, Pulokas J, Fellmann D, Cheng A, Guerra F, Quispe J, Staggs S, Potter CS, Carragher B (2005) Automated molecular microscopy: the new Legimon system. *J Struct Biol* 151: 41–60
- Tang S, Collier AJ, Elliott RM (1999) Alterations to both primary and predicted secondary structure of stem-loop IIIc of the hepatitis C virus 1b 5' untranslated region (5'UTR) lead to mutants severely defective in translation which cannot be complemented in trans by the wild-type 5'UTR sequence. *J Virol* 73: 2359–2364
- Terenin IM, Dmitriev SE, Andreev DE, Shatsky IN (2008) Eukaryotic translation initiation machinery can operate in a bacterial-like mode without eIF2. *Nat Struct Mol Biol* 15: 836–841
- Thakur A, Gaikwad S, Vijamarri AK, Hinnebusch AG (2020) eIF2 $\alpha$  interactions with mRNA control accurate start codon selection by the translation preinitiation complex. *Nucleic Acids Res* 48: 810280–810296
- Tivol WF, Briegel A, Jensen GJ (2008) An improved cryogen for plunge freezing. *Microsc Microanal* 14: 375–379
- Unbehaun A, Borukhov SI, Hellen CU, Pestova TV (2004) Release of initiation factors from 48S complexes during ribosomal subunit joining and the link between establishment of codon-anticodon base-pairing and hydrolysis of eIF2-bound GTP. *Genes Dev* 18: 3078–3093
- Wang J, Wang J, Shin BS, Kim JR, Dever TE, Puglisi JD, Fernández IS (2020) Structural basis for the transition from translation initiation to elongation by an 80S-eIF5B complex. *Nat Commun* 11: 5003
- Weisser M, Schäfer T, Leibundgut M, Böhringer D, Aylett CHS, Ban N (2017) Structural and functional insights into human re-initiation complexes. *Mol Cell* 67: 447–456
- Yamamoto H, Unbehaun A, Loerke J, Behrmann E, Collier M, Bürger J, Mielke T, Spahn CM (2014) Structure of the mammalian 80S initiation complex with initiation factor 5B on HCV-IRES RNA. *Nat Struct Mol Biol* 21: 721–727
- Yamamoto H, Collier M, Loerke J, Ismer J, Schmidt A, Hilal T, Sprink T, Yamamoto K, Mielke T, Bürger J et al (2015) Molecular architecture of the ribosome-bound hepatitis C virus internal ribosomal entry site RNA. *EMBO J* 34: 3042–3058
- Yokoyama T, Machida K, Iwasaki W, Shigetani T, Nishimoto M, Takahashi M, Sakamoto A, Yonemochi M, Harada Y, Shigematsu H et al (2019) HCV IRES captures an actively translating 80S ribosome. *Mol Cell* 74: 1205–1214
- Zheng A, Yu J, Yamamoto R, Ose T, Tanaka I, Yao M (2014) X-ray structures of eIF5B and the eIF5B-eIF1A complex: the conformational flexibility of eIF5B

- is restricted on the ribosome by interaction with eIF1A. *Acta Crystallogr D Biol Crystallogr* 70: 3090–3098
- Zheng SQ, Palovcak E, Armache JP, Verba KA, Cheng Y, Agard DA (2017) MotionCor2: anisotropic correction of beam-induced motion for improved cryo-electron microscopy. *Nat Methods* 14: 331–332
- Zivanov J, Nakane T, Forsberg BO, Kimanius D, Hagen WJ, Lindahl E, Scheres SHW (2018) New tools for automated high-resolution cryo-EM structure determination in RELION-3. *eLife* 7: e42166
- Zivanov J, Nakane T, Scheres SHW (2019) A Bayesian approach to beam-induced motion correction in cryo-EM single-particle analysis. *IUCr* 6: 5–17